

Full Length Article

Effect of Al^{3+} and Mg^{2+} on the flotation of fluorapatite using fatty- and hydroxamic-acid collectors – A multiscale investigation

Amir Eskanlou^a, Qingqing Huang^{a,*}, Yann Foucaud^{b,*}, Michael Badawi^c, Aldo H. Romero^d

^a Department of Mining Engineering, West Virginia University, Morgantown, WV 26506, USA

^b ICSM, Univ. Montpellier, CEA, CNRS, ENSCM, Marcoule, France

^c Laboratoire de Physique et Chimie Théoriques UMR CNRS 7019, Université de Lorraine, France

^d Department of Physics and Astronomy, West Virginia University, Morgantown, WV 26505-6315, USA

ARTICLE INFO

Keywords:

Fluorapatite
Metal ions
Flotation
Collector
Adsorption
DFT

ABSTRACT

Fluorapatite flotation is influenced by the dissolved lattice metal ions. Al^{3+} and Mg^{2+} from the associating gangue minerals influence the adsorption of collector molecules onto the fluorapatite surface during flotation. Hence, unveiling new insights on such interactions in the context of froth flotation at an atomic level paves the way for improving flotation selectivity. An original multiscale approach has been developed involving flotation experiments, electro-kinetic and adsorption density measurements, X-ray photoelectron spectroscopy studies, and density functional theory simulations. Fatty acid establishes an enhanced interaction with the bare apatite surface compared to the hydroxamates. Na^+ counter-ion contributes to the adsorption of fatty acid on bare apatite. Both Al^{3+} and Mg^{2+} ions are beneficial for the adsorption of fatty acid, thereby the fluorapatite flotation. For octanohydroxamic acid, the presence of Al^{3+} results in a stronger collector-apatite interaction, and therefore an enhanced flotation. For fatty acid and hydroxamates, adsorption of Mg^{2+} leads to an improved collector-apatite interaction. Benzohydroxamic acid is more vigorously adsorbed than octanohydroxamic acid in the presence of Mg^{2+} . Fatty acid establishes a stronger interaction with bare and $\text{Al}^{3+}/\text{Mg}^{2+}$ -treated fluorapatite, as opposed to hydroxamates. Mg^{2+} is more favorable than Al^{3+} in fluorapatite flotation using both fatty acid and hydroxamates.

1. Introduction

Apatite [$\text{Ca}_5(\text{PO}_4)_3(\text{OH}, \text{F}, \text{Cl})$] is the primary source for phosphorus (P), which is essential for the production of fertilizers that supplement the nutrition of many agricultural crops by providing a valuable source of phosphate [1]. Other important applications for apatite minerals are in biological science, as a possible host for the storage of nuclear waste, as a host for solid-state diode lasers, or in the development of P-containing compounds [1–3]. Besides, apatite generally contains significant amounts of strategic elements including rare-earth elements (REEs), uranium (U), and thorium (Th) and can therefore be used as a source for those elements [2,4]. Fluorapatite (FA) [$\text{Ca}_5(\text{PO}_4)_3\text{F}$] is the most well-characterized member of apatite group due to its large natural reserves [5]. The main gangue minerals that naturally coexist with FA are dolomite, quartz, and clays [6]. Froth flotation is the most efficient beneficiation technology for the separation of FA from its associated gangue minerals: more than 60% of the global marketable phosphate is

beneficiated via flotation [7,8].

Froth flotation is based on the modification of the surface physico-chemical properties of solid particles by the addition of chemical reagents to ultimately separate the valuable minerals from the gangues using air bubbles in an aqueous environment [9–11]. In phosphate flotation, fatty acids and their salts are commonly used as the collector, *i. e.*, the molecule that renders surfaces hydrophobic, due to their low cost and strong collecting ability [12]. Nonetheless, the high affinity of fatty acids for a large number of cations, including transition metals, alkali-earth elements, and REE, entails a lack of selectivity in the flotation process [7]. As an alternative to fatty acids, hydroxamic acids (HA) have recently drawn remarkable attention in phosphate flotation for their collecting ability and good affinity [13,14]. HA refers to a group of reagents capable of chelating with metallic atoms that have been successfully used for the flotation of clays, oxide copper, cassiterite, and other mineral types [15–19]. The separation efficiency in flotation strongly depends upon the selectivity during the adsorption process,

* Corresponding authors.

E-mail addresses: qingqing.huang@mail.wvu.edu (Q. Huang), yann.foucaud@univ-lorraine.fr (Y. Foucaud).

<https://doi.org/10.1016/j.apsusc.2021.151499>

Received 10 August 2021; Received in revised form 23 September 2021; Accepted 1 October 2021

Available online 5 October 2021

0169-4332/© 2021 Elsevier B.V. All rights reserved.

which itself is affected by a number of factors such as solution pH, differences in surface characteristics of associated minerals, selective functionality of chemical reagents, etc. [10].

To overcome the depletion of high-grade phosphate deposits associated with the growing global demand for P, valorization and reprocessing of the secondary resources are inevitable. Among the various known waste streams that can be considered as P-bearing secondary resources, waste clay (WC), a tailing of the phosphate ore process, presents a remarkable potential source for P as well as for other critical elements, e.g., REEs [20,21]. This stream is a dilute aqueous slurry (3–5 wt% solids) consisting of a mixture of clay minerals, silica sand, carbonates, FA, and other fine-grained minerals [22,23]. The flotation recovery of FA from secondary resources such as WC is subject to large difficulties that are generally attributed to the close similarities in composition and physicochemical properties of the coexisting minerals, slime-coating, unfavorable rheological properties of pulp, high gangue entrainment, and effect of dissolved lattice metal ions [6,7,24].

The presence of metal ions in the flotation environment can result from the water quality, the dissolution of host minerals, or the consumption of the grinding medium during the comminution process [25,26]. As such, in the flotation of FA from either high- or low-grade deposits, the presence of certain ions such as Ca^{2+} and Mg^{2+} is inevitable due to the presence of semi-soluble salt-type gangue minerals as dolomite and calcite [7]. This is further highlighted for low-grade secondary resources as WC, where not only the common phosphate minerals but also aluminum (Al)-rich phyllosilicates such as clays are present under an ultra-fine size, i.e., below 10 μm [23]. This very low particle size improves the mineral dissolution and, therefore, the release of various metal ions such as Al^{3+} into the flotation environment, which increases the complexity of the flotation process. In water, these ions can undergo various reactions, including hydrolysis, complexation, and adsorption. Such interactions can result in rendered surface charge of minerals, surface charge reversals, and therefore significantly affect the interactions between mineral surfaces and flotation reagents [27,28].

The nature and mechanisms of the above-mentioned interactions may be unique for each individual metal ion-mineral system. This still remains unraveled from various aspects for numerous cases of such systems in the context of froth flotation. Many studies have been devoted to investigating the influence of certain metal ions, e.g., Ca^{2+} and Mg^{2+} , on the flotation of FA using fatty acid collectors [29,30]. However, there is no consensus among the previous studies on the influence of these metal ions on the flotation of FA using fatty acids and the results are inconsistent in most cases. As few cases in point, Santos et al. [31], Al-Thyabat and Al-Zoubi [32], Elgillani and Abuozaid [33], and Sis and Chander [34] reported that Ca^{2+} and/or Mg^{2+} ions inhibit the flotation of phosphate minerals. In contrast, Al-Fariss et al. [29], Liu et al. [35], Ruan et al. [7], and Horta et al. [36] showed that an appropriate amount of Ca^{2+} and/or Mg^{2+} ions could improve the floatability of FA through enhanced collector adsorption. Moreover, the effect of other unavoidable lattice metal ions such as Al^{3+} on the flotation of FA has not been given the deserved attention yet. On overall, the interactions between mineral surfaces, metal ions, and flotation reagents are difficult to investigate by experimental techniques considering the atomic level of the involved mechanisms. Molecular dynamics simulations based on first-principles calculation techniques such as density functional theory (DFT) [37], known as *ab initio* molecular dynamics (AIMD) simulations, can be considered as powerful tools to unveil new insights on such interactions in the context of froth flotation at an atomic level [38,39]. Integrated approaches merging experimental observations with AIMD simulations are purported to be of significant value to help grasp the effect of the metal ions on the flotation of valuable minerals such as FA.

Mkhonto et al. [40] performed a series of DFT simulations in vacuum to investigate the adsorption of some organic molecules with various functional groups on different FA crystal surfaces. They demonstrated that the strongest interactions between reagents and FA surfaces are exhibited when the molecules are able to form multiple interactions

with surface Ca^{2+} ions. Besides, Xie et al. [41] investigated the interaction between fatty acid collectors and the (001) surface of FA by DFT calculations. They showed that the O atoms of fatty acid collectors establish a chemical bond with the Ca_1 site of the FA surface and that a hydrogen bond is formed between the H atom of the collector and the O atoms of a surface phosphate group. Moreover, many other studies [6,24,42–49] have been devoted to investigating the various properties of FA, e.g., electronic structure and floatability, surface complexation in hydrous form, and its surface electrical behaviors in the presence of Ca^{2+} and Mg^{2+} , as well as to exploring the adsorption mechanism of fatty- and hydroxamic acid collectors on FA.

The present study endeavored to investigate the interactions of fatty acid and hydroxamic acid collectors with FA in the presence or absence of Al^{3+} and Mg^{2+} metal ions. For this purpose, we combined atomistic simulations with zeta potential measurements, XPS studies, adsorption density measurements, and micro-flotation tests. We aimed at unraveling how the presence of those metal ions influences the adsorption of the aforementioned collectors on the FA surface, and thereupon the flotation selectivity.

2. Materials and methods

2.1. Crystal structure and solubility of FA

FA, mainly composed of calcium fluoro-phosphate, has a hexagonal di-pyramidal crystal system in the space group $\text{P6}_3/\text{m}$, with $a = b = 9.224 \text{ \AA}$ and $c = 6.805 \text{ \AA}$ and $\alpha = \beta = 90^\circ$ and $\gamma = 120^\circ$ [50]. The crystal structure of FA is presented in Fig. S-1 of the [supplementary material](#) (Appendix A). The structure of FA consists of individual orthophosphate tetrahedra linked by Ca cations. The orthophosphate groups form the skeleton with two types of Ca sites; first, the $[\text{Ca}_1]$ site is occupied by four Ca atoms in a nine-fold coordination, while the second $[\text{Ca}_2]$ site is occupied by six Ca atoms in a seven-fold coordination. Fluoride (F^-) anions are located within the same channels as the Ca_2 sites and usually have a high mobility [51,52]. Thus, the FA structure contains Ca–F, Ca–O, and P–O bonds; the consideration of the relative electrostatic strength of these bonds suggests that their relative destruction rate is consistent with: $\text{Ca–F} > \text{Ca}_1\text{–O} > \text{Ca}_2\text{–O} > \text{P–O}$. Considering its structure, once all Ca–F and Ca–O bonds are broken, FA is destroyed, while breaking P–O bonds (1) requires too much energy and (2) is unnecessary for FA dissolution [51,53,54]. The most abundant crystal faces of FA formed during the cleavage process are the (001), (100), (101), and (111) surfaces [53,54].

Although apatite-group minerals are generally considered as semi-soluble salt-type minerals, FA is a highly insoluble calcium phosphate compared to other apatite-group minerals, i.e., hydroxyapatite and chlorapatite. The solubility product of stoichiometric FA at 37 °C is $3.19 \pm 0.14 \times 10^{-61} \text{ mol}\cdot\text{L}^{-1}$ as reported by Moreno et al. [55]. A suggested explanation for this very low solubility product is that cohesive forces are relatively stronger in FA due to its smaller unit-cell dimensions compared to hydroxyapatite and chlorapatite [56,57]. Fig. 1 shows a schematic representation of surface protonation of apatite at different solution pH ranges, where the adsorption of protons onto negatively charged O ions of the orthophosphate group surfaces is depicted. This process is referred to as the hydrogen catalytic dissolution model for apatite [51,58]. Recent computer simulations have revealed that, in the case of FA, F^- ions located on the surface are poorly protonated, and that these ions exhibit $\text{pK}_\text{B} = 10.8$, which indicates a weak base [59].

The Ca^{2+} in FA can be substituted by REEs, e.g., cerium (Ce), lanthanum (La), and yttrium (Y), via a charge-balancing coupled substitution, resulting in lattice defects that exert a considerable influence on the FA surface properties [60]. The presence of REE impurities makes FA receive electrons more readily and hence increases its oxidation ability, especially when a reductive collector, e.g., fatty acid, is employed [60,61].

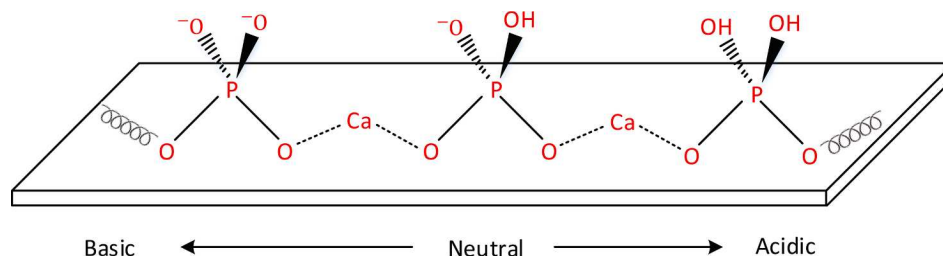


Fig. 1. A schematic representation of surface protonation of apatite at different solution pH values (reproduced from [51]).

2.2. Materials and chemicals

For the experiments, pure FA was purchased from Ward's Science (USA). Analytical X-ray powder diffraction (XRD) in the 2θ range of $10\text{--}100^\circ$ and Cu-K α radiation ($\lambda = 1.5406 \text{ \AA}$) was employed to investigate the crystalline phases and mineral associations. The morphological characteristics of the sample were investigated using scanning electron microscopy (SEM) coupled with energy-dispersive X-ray spectroscopy (EDS), which allows for targeted analysis of sample surfaces. Inductively coupled plasma mass spectrometry, *i.e.*, ICP-MS method was employed for the elemental characterization of the sample. The particle size distribution (PSD) was measured for the representative samples using a CILAS 1190 particle size analyzer.

In the current study, octanohydroxamic acid (OHA), benzohydroxamic acid (BHA), and sodium oleate (NaOl) were used as the collectors for the FA flotation. Methyl isobutyl carbinol (MIBC) was used as the frothing agent in all the flotation experiments. Hydrochloric acid (HCl) and sodium hydroxide (NaOH) solutions of relevant concentrations were used as pH regulators. Magnesium chloride (MgCl₂) and aluminum chloride (AlCl₃) were used to prepare multivalent metal solutions. Iron (III) chloride (FeCl₃) was used for preparing the ferric solution for the coloring of hydroxamates in UV-Vis spectroscopy. A solution of potassium chloride (KCl) at $1 \times 10^{-3} \text{ mol}\cdot\text{L}^{-1}$ was used as the supporting electrolyte for zeta potential measurements. Potassium nitrate (KNO₃) was used as the indifferent background electrolyte for the adjustment of the ionic strength (IS) of the synthetic metal solutions. Details of the chemicals used in the present study are listed in Table S-1 of the [supplementary material](#). Milli-Q deionized (DI) water (18.2 M Ω -cm) was used for the stock solution preparations, zeta potential and adsorption density measurements, as well as for micro-flotation experiments.

Stock solutions of 1×10^{-5} , 1×10^{-4} , and $1 \times 10^{-3} \text{ mol}\cdot\text{L}^{-1}$ of Mg²⁺ and Al³⁺ were prepared by dissolving the appropriate amount of their corresponding chloride salts using DI water. The IS of all synthetic solutions was adjusted to $2 \times 10^{-3} \text{ mol}\cdot\text{L}^{-1}$ using KNO₃ as an indifferent background electrolyte. Solution pH was adjusted using a $1 \times 10^{-1} \text{ mol}\cdot\text{L}^{-1}$ NaOH and diluted HCl solutions.

2.3. Characterization techniques

2.3.1. Zeta potential measurements

The possible surface potential changes of FA induced by the absence or the presence of Mg²⁺ and Al³⁺ metal ions were approximated by the changes in zeta potential, which can approximate the surface potential based on the potential measured at the slipping plane. The surface charge can be affected by the charge balance (charge reduction, neutralization, or reversal) in the electrical double-layer (EDL); divalent or trivalent cations strongly compress the EDL, which affects the measured zeta potential value [62]. The compression of the EDL with the ionic strength [$IS = \frac{1}{2} \sum C_i z_i^2$ (z , ion valence, and C_i , ion concentration)] is described by the Debye length (λ_D , thickness of the EDL) [62,63]. In flotation conditions, one usually controls the concentration of ions, which affects the Debye length and, therefore, the zeta potential of the minerals. We compared the zeta potential of FA with a constant

concentration of Mg²⁺ or Al³⁺ ($1 \times 10^{-3} \text{ mol}\cdot\text{L}^{-1}$) as a function of pH with a background electrolyte (KCl) concentration of $1 \times 10^{-3} \text{ mol}\cdot\text{L}^{-1}$ [28]. The procedure employed for the measurement of zeta potential is described in the [supplementary material](#).

2.3.2. XPS measurements

For XPS analyses, three different solutions at 1×10^{-3} , 1×10^{-4} , and $1 \times 10^{-5} \text{ mol}\cdot\text{L}^{-1}$ of AlCl₃ and MgCl₂ at pH 9 were prepared and were used to condition 0.5 g of pure FA for 24 h, under agitation provided by a magnetic stirrer. After the conditioning stage, the treated powder samples were thoroughly rinsed with DI water and then placed in a desiccator under partial vacuum for overnight soft drying prior to being subjected to the XPS analysis [64]. XPS measurements were performed using a Physical Electronics PHI 5000 VersaProbe system. The system was equipped with a monochromatic Al K- α X-ray source at 1486.6 eV with a 100 μm beam size. All XPS measurements were carried out at room temperature and at a pressure below 10^{-7} Torr. Compositional survey scans were obtained using a pass energy of 117.4 eV and energy step of 0.5 eV. High-resolution, detailed scans of each element were acquired using a pass energy of 23.5 eV and an energy step of 0.1 eV. The obtained binding energies were calibrated using standard carbon peak C 1s for C-C at 284.8 eV [65] and were fitted using Thermo Advantage 4.60 (Thermo Fisher Scientific Inc., USA) software.

2.4. Adsorption density measurements

The adsorption of NaOl, BHA, and OHA on FA under various conditions was investigated by the adsorption-from-solution technique, which consists in measuring the difference of the collector concentration in the solution before and after contact with the FA sample. The detailed procedure for the measurement of adsorption densities is provided in the [supplementary material](#).

2.5. Atomistic simulations

As the starting point for the atomistic simulations, a primitive cell of Ca₅(PO₄)₃F was generated based on the American Mineralogist Crystal Structure Database (AMCSD) [66], which reported lattice parameters of $a = b = 9.37 \text{ \AA}$ and $c = 6.88 \text{ \AA}$ with $\alpha = \beta = 90^\circ$ and $\gamma = 120^\circ$. All the DFT simulations were performed using the Vienna Ab initio Simulation Package (VASP), version 5.4.4 [67]. The semi-local exchange-correlation functional of Perdew-Burke-Ernzrhof (PBE) in the general gradient approximation (GGA) [68] was employed. The Kohn-Sham equations [69] were solved self-consistently [70] with an energy convergence criterion of 10^{-6} eV . The electron-ion interactions were described using the Projected Augmented Wave (PAW) method [71]. To help the electronic convergence, a Methfessel-Paxton smearing [72] of $\sigma = 0.1 \text{ eV}$ was applied. For static calculations, the structural relaxations were conducted until all forces were smaller than $0.03 \text{ eV}\cdot\text{\AA}^{-1}$.

The FA primitive cell was fully relaxed (in terms of ion positions, cell size, and cell shape) using a cut-off energy of 450 eV and a k -points grid of $2 \times 2 \times 2$ [73], based on the plane wave cut-off kinetic energy and k -points convergence tests results presented in Fig. S-3. The optimized lattice parameters of the relaxed unit cell were $a = b = 9.46 \text{ \AA}$, $c = 6.89$

Å, and $\alpha = \beta = 90^\circ$, $\gamma = 120^\circ$, which were in very good agreement with the experimental values. Then, from the fully-relaxed unit cell, a FA slab of $a \times b \times c = 2 \times 2 \times 1$ comprising a total number of 168 atoms was generated, as shown in Fig. 2. The (001) surface, which represents the most exposed and stable, *i.e.*, with the lowest surface energy, surface of FA [3,5,41,44,74], was built by adding vacuum along the *c*-axis. To avoid any unwanted interaction with the periodic images, a vacuum thickness was set above the uppermost atom along the *c*-axis of the supercell. Different values were tested during preliminary calculations, from 10 Å to 20 Å, and this latter was selected (Fig. 3). For all the simulations involving the supercell, due to its large size, the Γ -point only was employed for sampling the Brillouin zone.

To avoid the influence of the initial position of the ions and molecules on their adsorption structure, AIMD simulations were performed for each system prior to the energy calculation. AIMD simulations combine the accuracy of DFT with the movement of atoms and the pressure/temperature control allowed by MD simulations, since, at each time step, the forces are calculated by DFT. During the AIMD simulations, the atoms moved significantly to spontaneously form the most stable configurations and we observed that all the considered input configurations consistently led to the same final geometries. Hence, we obtained the most stable atomic structure of the system, and therefore we could discuss the adsorption mechanisms. The temperature was set to 300 K and a Nosé-Hoover thermostat [75–77] was used. A time step of 1 fs was employed and 40,000 steps were realized to reach a total simulation time of 40 ps. The corresponding adsorption energies were determined by static DFT calculations conducted on the most stable configuration extracted from the AIMD simulations. For all the AIMD simulations, a set of 20 atoms including 8 Ca and 12 O atoms at the bottom layer of the supercell were frozen to the bulk positions to avoid any unwanted drift of the FA slab. The adsorption energies of the metal ions (considered by their hydrolysis products), of the collector on the bare surface, and of the collector on the surface activated by the hydrolysis products of the metal ions were determined based on Eq. (1), (2) and (3), respectively [41]:

$$(\Delta E_{\text{ads}})_{\text{Ion}} = E_{(\text{Slab}+\text{Hydrolysis product})} - E_{(\text{Slab})} - E_{(\text{Hydrolysis product})} \quad (1)$$

$$(\Delta E_{\text{ads}})_{\text{Collector}} = E_{(\text{Slab}+\text{Collector})} - E_{(\text{Slab})} - E_{(\text{Collector})} \quad (2)$$

$$(\Delta E_{\text{ads}})_{\text{Collector-Activated}} = E_{(\text{Slab}+\text{Hydrolysis product}+\text{Collector})} - E_{(\text{Slab}+\text{Hydrolysis product})} - E_{(\text{collector})} \quad (3)$$

where the energies correspond to the potential energies computed by static DFT calculations conducted on snapshots extracted from the AIMD simulations. Three collectors were investigated in the current study, *i.e.*, BHA and OHA, the cyclic and straight-chain HA collector, respectively, and NaOl. For the AIMD simulations, in order to reduce the computational cost, sodium octanoate (SC) was used instead of NaOl since they have the same functional group and the chain length does not affect significantly the adsorption of a single molecule [78]. Considering the pK_a values of the collectors (BHA: ~ 8.6 [79], OHA: ~ 9.5 [49], NaOl: 4.9 [80]), at pH = 9, BHA and OHA are present in both their neutral and anionic forms, while fatty acids are present only in their anionic form. Therefore, in our AIMD simulations, HA were investigated in both neutral and anionic forms, while SC was considered only in its anionic form. The three molecules are presented in Fig. 4 in their free anionic form.

To obtain the most stable forms of Al^{3+} and Mg^{2+} under the flotation conditions, *i.e.*, at pH = 9, $C_{\text{Tot}} = 1 \text{ mol}\cdot\text{L}^{-1}$, $p\text{CO}_2 = 10^{-3.5} \text{ atm}$ at 1 atm, and $T = 25^\circ\text{C}$, we built speciation diagrams for the two ions using Medusa-Hydra chemical equilibrium software [81], presented in Fig. 5. According to these latter, the hydrolysis products of Al^{3+} and Mg^{2+} ions at the target conditions are $\text{Al}(\text{OH})_3$ and MgCO_3 , respectively. Therefore, $\text{Al}(\text{OH})_3$ and MgCO_3 were considered in the atomistic simulations for Al^{3+} and Mg^{2+} species, respectively, and were generated using IQmol software [82], as presented in Fig. 5. Besides, Avogadro software [83] was employed to import and place the target collector molecule(s) and/or metal ion species into the vacuum space at a minimum distance of 2.5 Å above the uppermost atoms on the surface of the FA slab. Both vertical and flat input configurations of the molecules on the surface were explored to assess the most favored adsorption mode, although they all led to the same final geometries during the AIMD simulations. The presence of Na^+ ions is inevitable in the flotation environment due to the pH adjustment using NaOH. In addition, the counter-ion plays a crucial role in the adsorption process via initiating the formation of the surface layer, and in stabilizing the adsorption of the free anionic collector molecule [84]. Therefore, and to keep the electric neutrality in the cell, a Na^+ was systematically added as the collector counter-cation and placed at a distance of 5 Å from the anionic molecule. The role of the sodium counter-ion in the adsorption of the target collector molecules was also investigated on both bare and activated FA surfaces. VESTA molecular visualization software [85] was used for generating the slab as well as

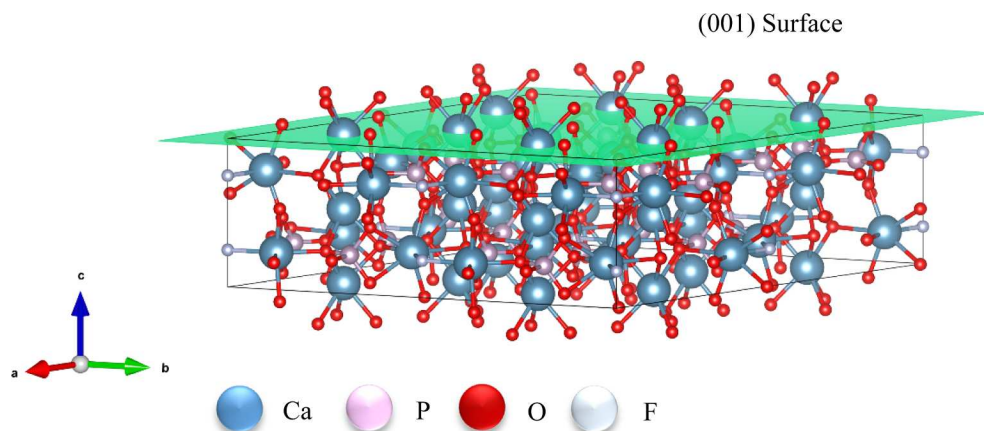


Fig. 2. The FA mineral unit-cell and slab used for the current study.

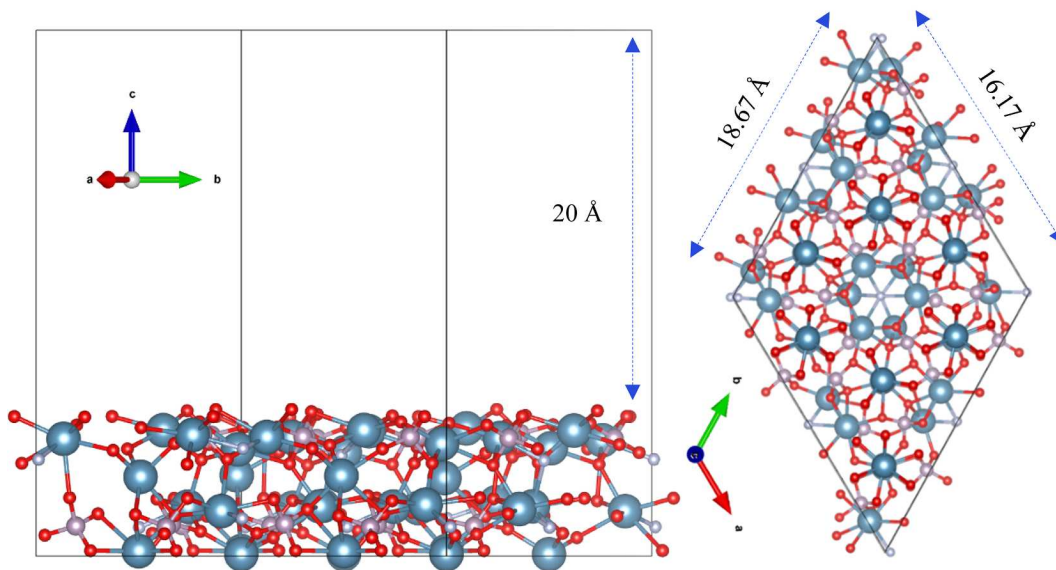


Fig. 3. The dimensions of FA supercell employed for the current study.

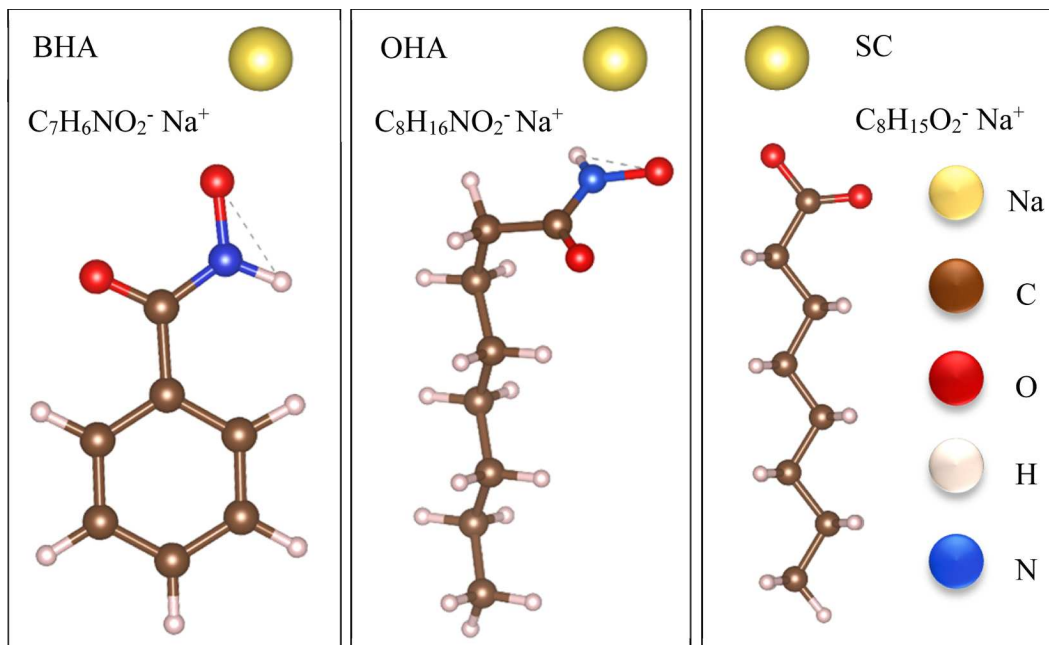


Fig. 4. Molecular models of the target collectors in their free anionic forms.

visualizing the ultimate configurations obtained from AIMD simulations.

2.6. Micro-flotation experiments

The micro-flotation experiments were conducted on the +38–53 μm size fraction of FA powder. Flotation tests were performed using a ~ 75 mL modified Partridge-Smith micro-flotation cell (Fig. S-4 of the [supplementary material](#)). For each experiment, 1 g of dried powder sample was placed in a glass beaker containing 50 mL DI water with an adjusted pH value, stirred using a magnetic stirrer and a magnet bar. The pH of the solution was readjusted to the desired value prior to the addition of the flotation reagents, which were added sequentially. Each reagent was conditioned for ~ 2 min at room temperature, followed by the addition of the frothing agent (20 ppm, *i.e.*, 1.95×10^{-4} mol·L $^{-1}$), which

continued to be conditioned for 1 more minute. The suspension pH was monitored and maintained. The ultimate suspension was then transferred into the flotation cell mounted on top of a magnetic stirrer, using an extra 25 mL of pH-adjusted DI water. To keep material in suspension inside the cell, a magnet bar was placed directly on top of the frit. The flotation process was carried out for 1 min by injecting the gas at a flowrate of 30 mL·min $^{-1}$. Pure nitrogen (N $_2$) gas was employed instead of lab air to eliminate carbonate precipitation in the solution due to CO $_2$ interference. Synthetic metal ion solutions of 1×10^{-3} mol·L $^{-1}$ MgCl $_2$ or AlCl $_3$ were used as the base solution for the experiments that aimed to investigate the effect of the metal ions on the flotation of FA. Floated and non-floated fractions were collected, dried, weighed, and analyzed to calculate the mineral grade and recovery. The reported result for each flotation experiment is the mean value of three replicate tests.

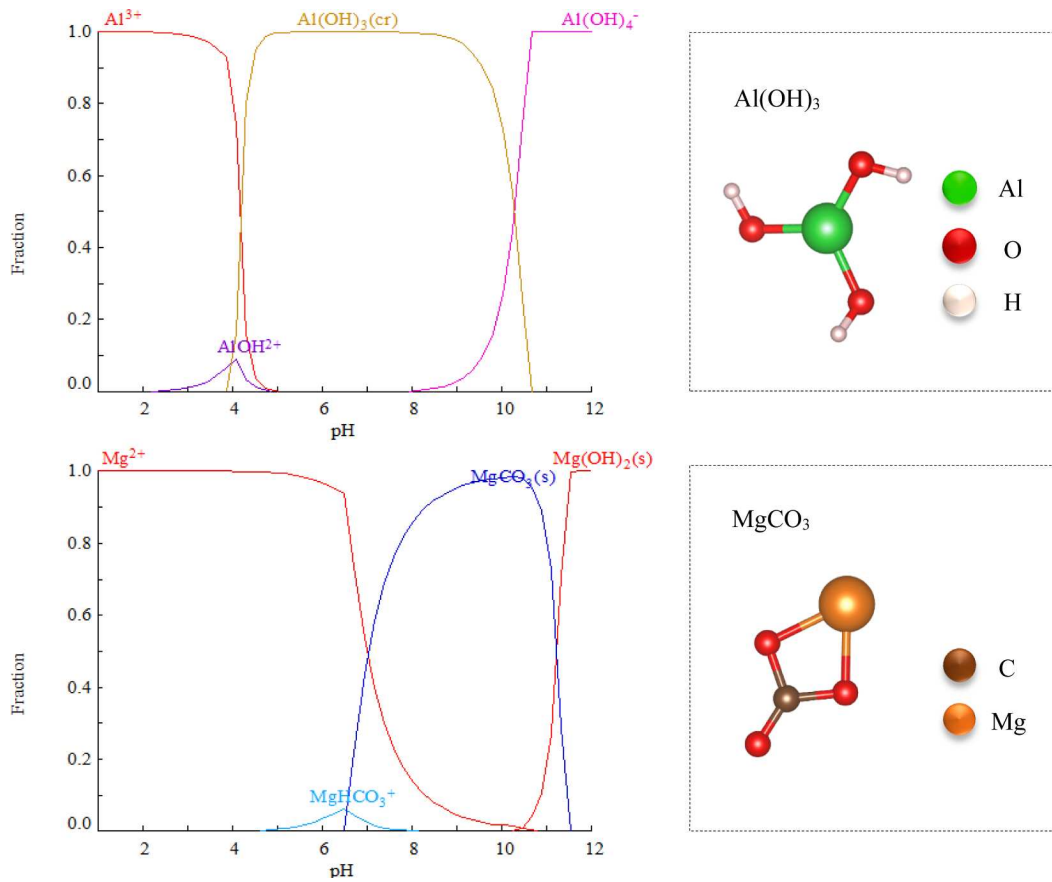


Fig. 5. Speciation diagrams of Al^{3+} and Mg^{2+} ions in water; total concentration: $[\text{Al}^{3+}]_{\text{TOT}} = 1.0 \text{ mM}$, $[\text{Mg}^{2+}]_{\text{TOT}} = 1.0 \text{ mM}$, $p\text{CO}_2 = 10^{-3.5} \text{ atm}$ at 1 atm and $T = 25 \text{ }^\circ\text{C}$.

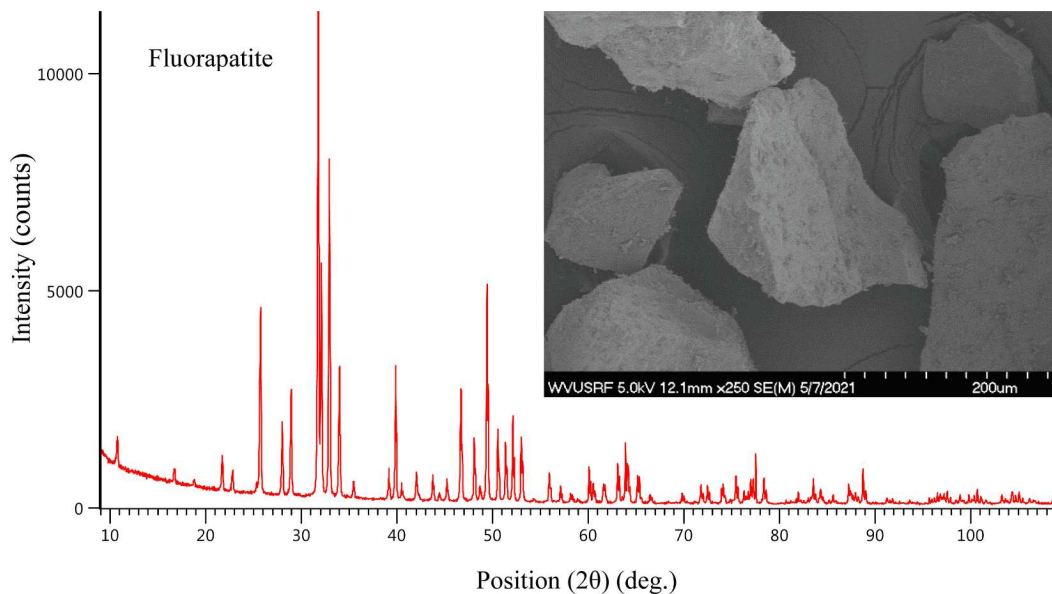


Fig. 6. X-ray powder diffractogram and SEM micrograph of the pure FA sample used for the current study.

3. Results and discussion

3.1. Material characterization

The XRD and SEM, and elemental characterization results are presented in Fig. 6 and Table 1, respectively. The morphological

characterization showed that the FA particles had irregular shapes. It can be seen from Table 1 that Ca, P and not-detectable elements, *i.e.*, F and O accounted for the major components of the FA, corresponding to a total of 96.5 wt%. Other elements, including Si, Ce, Th, La, etc., were also detected in negligible amounts.

Table 1

Elemental composition (ICP-MS results) of the FA mineral sample (ND refers to not detectable).

Mineral	Composition	wt.%/ppm	Composition	ppm
Fluorapatite	ND	36.90 (%)	Mg	193
	Ca	40.20	Gd	191
	P	19.40	U	153
	Si	0.93	Dy	85
	S	0.65	Zn	50
	Ce	0.58	Er	43.9
	Th	0.38	Eu	31
	La	0.27	Yb	29.3
	Nd	0.23	Tb	18.3
	Fe	0.10	Ho	14.9
	Al	751 (ppm)	Cl	11
	Pr	605	Tm	5
	Mn	503	Lu	3.8
	Y	415	Co	1.9
	Sm	261	Sc	1
	Ni	257		

ND: not detectable (F and O).

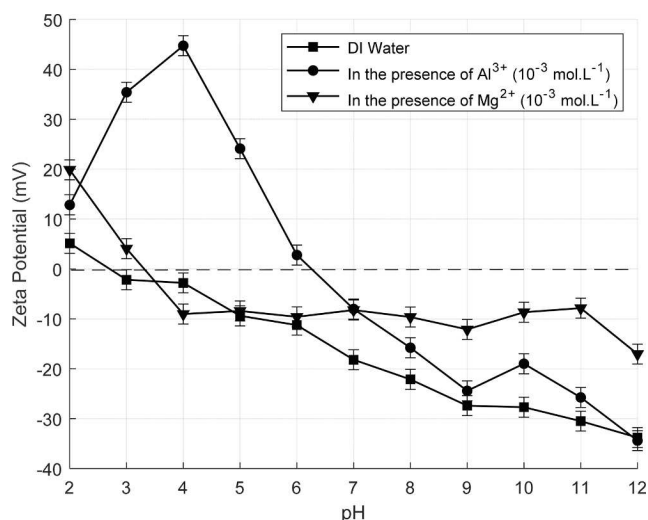


Fig. 7. Zeta potential of FA as a function of solution pH in the presence and absence of Al^{3+} and Mg^{2+} .

3.2. Effect of Al^{3+} and Mg^{2+} on zeta potential of FA

The evolution of the zeta potential of FA as a function of the solution pH is compared for the three different scenarios, *i.e.*, FA in DI water, in $1 \times 10^{-3} \text{ mol.L}^{-1} \text{ Mg}^{2+}$, and in $1 \times 10^{-3} \text{ mol.L}^{-1} \text{ Al}^{3+}$ with λ_D values of 9.64 nm, 5.57 nm, and 4.11 nm, respectively, considering $10^{-3} \text{ mol.L}^{-1}$ KCl as the background electrolyte (Fig. 7) [86,87]. The presence of the metal ions results in a change in the zeta potential of FA, slightly in the case of Mg^{2+} and significantly for Al^{3+} , which is consistent with the compression of the EDL induced by the change in ionic strength. The isoelectric point of FA shifts from around 3 for the bare mineral to 3.5 and 6.5 in the presence of Mg^{2+} and Al^{3+} , respectively. Within the pH range of 3 to 6.5, the zeta potential of FA tends to be positive in the presence of Al^{3+} metal ions compared to the bare mineral, while this range is significantly tighter in the case of Mg^{2+} , *i.e.*, pH 3 to pH 3.5. Such changes in the zeta potential values can be attributed to the compression of the EDL under high IS conditions [88]. This could be ascribed to the adsorption of the hydrolysis species of the metal ions on the mineral surface [7]. It is also shown that the presence of the metal ions does not cause overcharging in the EDL or electro-kinetic charge reversal on the FA surface [28].

3.3. XPS measurements

The surface composition of FA was determined before and after being conditioned with the metal ions. The results are presented in the form of survey spectra, high-resolution spectra, and atomic concentrations of various elements on the surface, in Fig. S-5 of the supplementary material, Fig. 8 and Table 2, respectively. The survey spectra (Fig. S-5) show the major characteristic peaks of the elements present at the bare FA mineral surface, which are C, O, Ca, P, and F. Comparing the survey

Table 2

FA surface composition after treatment with solutions of various $\text{MgCl}_2/\text{AlCl}_3$ concentrations.

Dosage (mol L^{-1})	Apatite surface composition (at.%)						
	C	O	F	Mg	Al	P	Ca
Bare FA	13.6	54.6	4.0	0	0	11.1	16.8
10^{-5} MgCl_2	13.9	51.2	4.9	1.5	0	11.7	16.8
10^{-4} MgCl_2	14.5	51.8	4.9	2.5	0	10.7	15.6
10^{-3} MgCl_2	16.1	52.3	3.1	4.3	0	10.0	14.2
10^{-5} AlCl_3	12.9	53.8	3.7	0	2.5	11.1	16.0
10^{-4} AlCl_3	12.4	57.0	2.9	0	7.9	8.8	11.1
10^{-3} AlCl_3	12.0	61.7	1.6	0	16.6	4.1	4.0

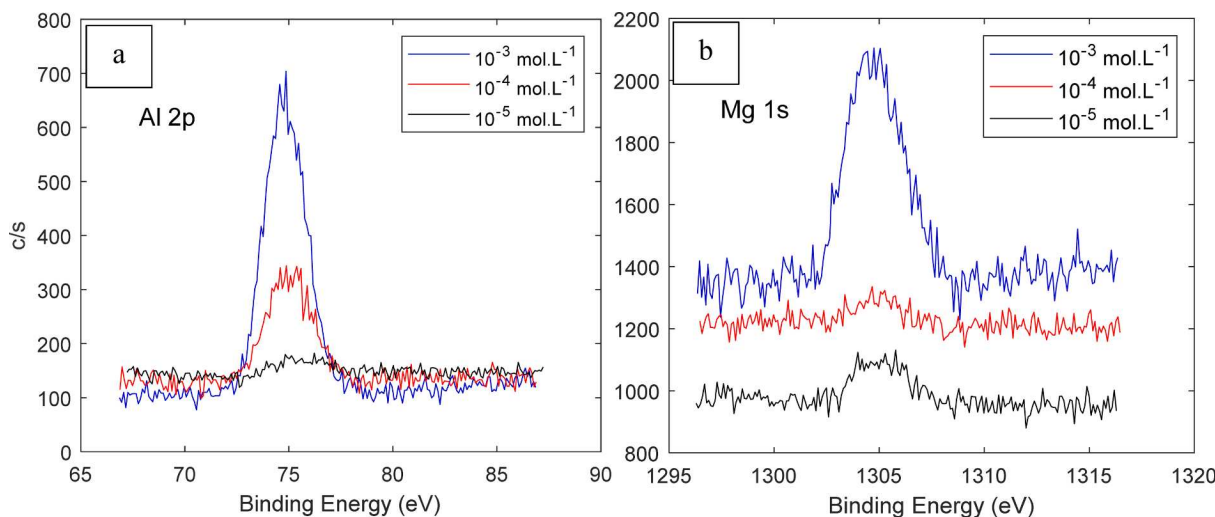


Fig. 8. XPS spectra of FA at various concentrations of (a): Al^{3+} , and (b): Mg^{2+} metal ions.

spectra for the bare and Al/Mg-treated mineral surface, the peak locations of Al 2p at 74.9 ± 0.1 eV and Mg 1s at 1304.9 ± 0.1 eV obtained from the detailed XPS scans suggest the adsorption of Al^{3+} and Mg^{2+} via Al—O and Mg—O bonds [89]. The detailed high-resolution Al 2p and Mg 1s peaks in Fig. 8 show that the amount of the metal ions adsorbed onto the mineral surface increases with an elevated concentration of these ions in the solution. This is further supported by semi-quantitative XPS-determined surface atomic compositions of the FA treated with different concentrations of the metal ions, as presented in Table 2. It is also seen from Table 2 that, in conformity with the increase in the amount of Mg atoms identified on the mineral surface, the amount of C and O atoms increases as well. This supports the adsorption of Mg^{2+} on the FA surface under MgCO_3 form. Similarly, consistent with the increase in the amount of Al atoms adsorbed on the mineral surface, the amount of O identified on the surface also increases, which supports the adsorption of Al^{3+} under its hydroxide form. One noteworthy fact here is that in order for the electro-neutrality of the mineral surface to be met, the adsorption of metal ions is necessarily accompanied by the adsorption of their counter-ions [90]. From a thermodynamic perspective, under the given physicochemical condition, *i.e.*, pH 9, free metal ions in the solution react with carbonate or hydroxide ions forming MgCO_3 or $\text{Al}(\text{OH})_3$ species, which are probably adsorbed on the mineral surface during treatment. Hence, the increased presence of C and O on the mineral surface can be explained by the adsorption of the metal ions in the form of their hydrolysis products. Another striking point that can be inferred from Table 2 is that at 1×10^{-3} mol L⁻¹ concentration, Al^{3+} species almost fully coat the mineral surface so that the concentrations of the FA lattice elements, *i.e.*, Ca, P and F drop from 16.8, 11.1 and 4.0 % on the bare surface to 4.0, 4.1 and 1.6 % on the treated surface, respectively. For the Mg-treated surface, the concentrations of Ca, P and F drop to 14.2, 10 and 3.1 % on the treated surface, respectively. Moreover, the Ca/P and Ca/F ratios for the bare surface are obtained as 1.51 and 4.2, respectively. Considering the chemical formula of FA, however, these ratios should be 1.66 and 5, respectively. Such discrepancy could be attributed to the primary washing of the pure mineral sample with a diluted acidic solution (2.5 vol% H_2SO_4) to ensure that the particles were free of any contamination. For the treated mineral surface (Al/Mg concentration of 10^{-3} mol.L⁻¹), similarly, Ca/P and Ca/F ratios are respectively obtained as 1.42 and 4.58 for Mg-treated surface, and 0.98 and 2.5 for Al-treated surface. The deviation of the ratios from those obtained for the bare mineral could obviously be attributed to the substitution of the surface Ca^{2+} ions with Mg^{2+} and Al^{3+} .

3.4. Adsorption density measurements

The adsorption density measurement results are presented in Fig. 9. The adsorption density for the three considered collectors on the FA mineral surface changes in the order of Mg^{2+} -treated FA > Al^{3+} -treated FA > bare FA. This suggests that the adsorption of both fatty acid and HA collectors on the FA mineral surface is favored by the presence of Mg^{2+} and Al^{3+} metal ions, with however a higher effect of the former compared to the latter. For BHA adsorption on Al^{3+} -treated mineral surface, however, the adsorption density exhibits a very slight (almost negligible) increase as opposed to the bare mineral surface. This could be due to the poor tendency of BHA to interact with Al^{3+} at the mineral surface. This will be further discussed later in the following sections.

The differences in the amounts of the three collectors adsorbed on the bare mineral surface could be attributed to the coexistence of the neutral and anionic forms of HA collectors at pH 9. Such coexistence can induce a stabilization of the adsorption layer by reducing the polar repulsions between the polar groups of the collector molecules while maintaining strong chain-chain lateral interactions. This generally results in a more compact layers of adsorption on the surface compared to fatty acid, which is only present in its anionic form at pH 9 [91]. As well, such difference in the adsorption amount of the different collectors could owe to the difference in the packing area of the molecules that induce the compacity of the adsorption layers [92,93]. On overall, after the adsorption of the $\text{Al}^{3+}/\text{Mg}^{2+}$ species on the surface, the formation of new adsorption sites are induced, which reduces the polar repulsion between collector functional heads. Hence, the adsorption layer is tightened resulting in a higher adsorption density of collectors, as indicated in Fig. 9.

3.5. Atomistic simulations

Adsorption configurations of SC, BHA, and OHA molecules in their free anionic forms accompanied by the sodium counter-ion on bare and $\text{Al}^{3+}/\text{Mg}^{2+}$ -treated FA (001) surfaces are presented in Fig. 10. It is shown that SC, as the fatty acid molecule, adsorbs on the mineral surface through a bidentate bonding of O^{2-} atoms of the carboxyl group (COO^-) to the Ca^{2+} cationic sites (Ca—O : 2.21 Å) along with a Na^+ -mediated O—O bonding. This indicates that Na^+ counter-ion contributes to the adsorption of fatty acid on the FA surface through mediating the O—O bonding between the molecule and the mineral surface. For the hydroxamates, *i.e.*, BHA and OHA, a mono-dentate bonding of an O^{2-} atom of

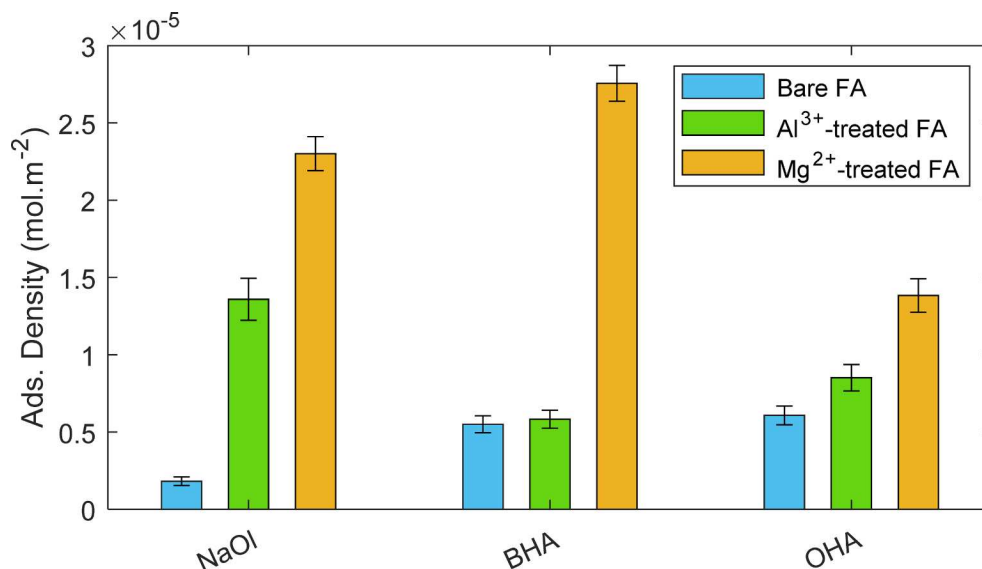


Fig. 9. Adsorption densities of NaOI, BHA, and OHA collectors in the presence and absence of the metal ions.

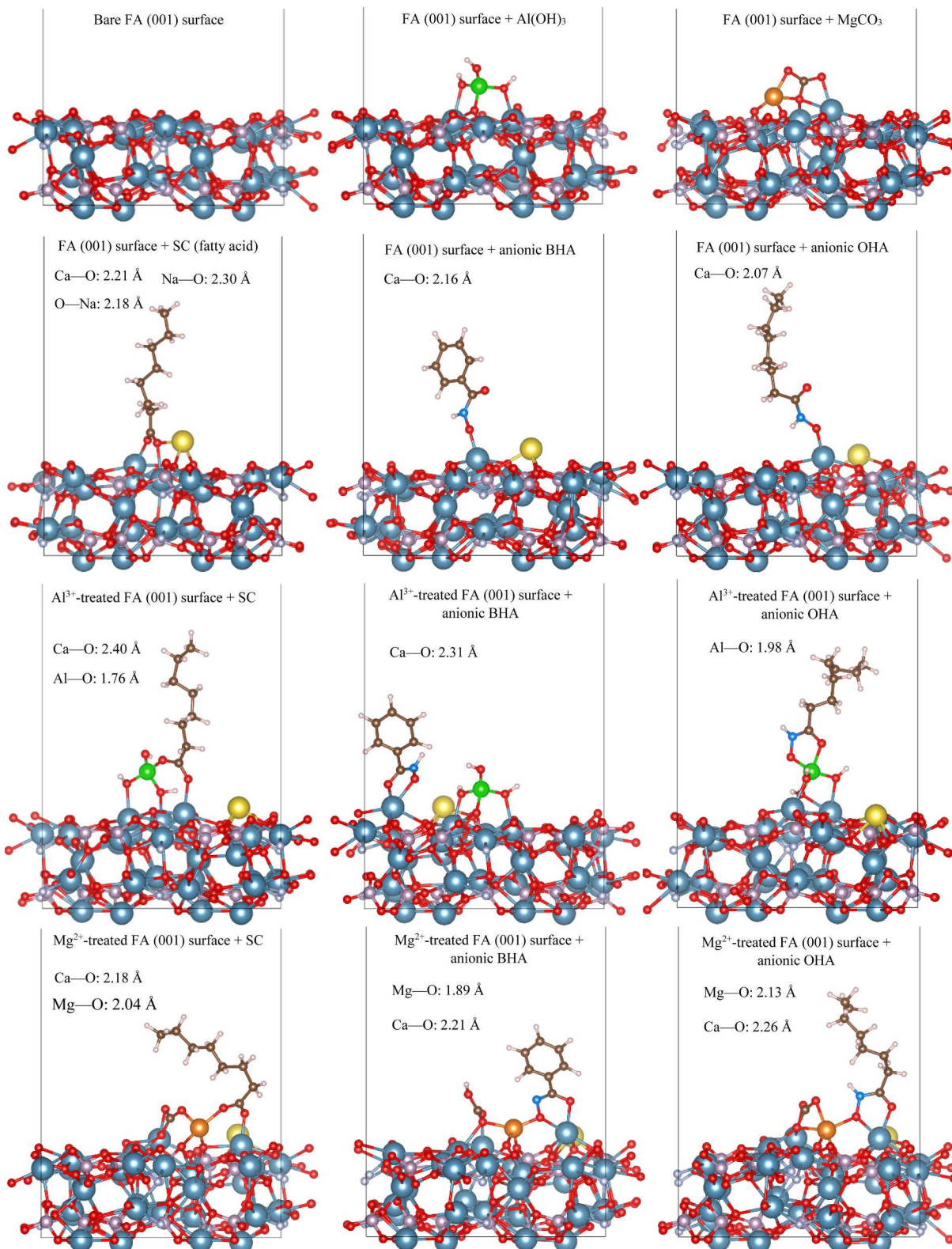


Fig. 10. Adsorption configurations of the fatty- and hydroxamic acid collectors on bare and Al³⁺/Mg²⁺-treated FA (001) surfaces.

the HA to a Ca²⁺ cationic site (BHA: Ca—O: 2.16 Å, OHA: Ca—O: 2.07 Å) is established. Unlike for SC, the Na⁺ ion does not contribute to the adsorption of the HA molecules on the bare FA surface. For chelating collectors, the adsorption on mineral surfaces is known to be a frontier-orbital-controlled reaction, accompanied by charge transfer or covalent/coordination bond formation [94]. Fatty acid collectors are well known

to interact strongly in their carboxylate form with Ca²⁺ ions at the mineral surface and in solution [42]. As the result of such interaction, the carboxylate molecule forms a mono/multi-layer of Ca-dicarboxylate on the surface depending on its concentration in the solution [42,88,95]. Such adsorption of fatty acid molecules on Ca-bearing mineral surfaces is believed to occur under chemisorption mechanism, as well-

Table 3
The adsorption energy of different collector molecules and species on FA (001).

Reagent/Species	Substrate	Ads. Energy (kJ mol ⁻¹)	
SC	Bare (001) FA surface	-392.7	
BHA		-235.4	-80.2
OHA		-176.3	-48.0
Al(OH) ₃	Al ³⁺ -treated (001) FA surface	-171.9	
MgCO ₃		-280.0	
SC		-431.4	
BHA	Mg ²⁺ -treated (001) FA surface	-295.8	-156.1
OHA		-355.2	-201.5
SC		-589.5	
BHA		-485.9	-293.4
OHA		-436.4	-257.2

documented in the literature [36,41,42,48,84]. The adsorption energies of SC, BHA, and OHA molecules on the bare FA surface were -392.7, -235.4, and -176.3 kJ·mol⁻¹, respectively, as presented in Table 3. This indicates that SC establishes stronger and more favorable chemisorption (more negative binding energy) with the FA surface compared to the HA collectors and, therefore, that SC exhibits a relatively stronger chelating ability with Ca²⁺ FA surface lattice metal ions [96,97]. This is further supported by the relatively shorter Ca—O bond length obtained for SC adsorption. Such stronger interaction of SC molecule with the FA surface could also be linked to the preferential contribution of sodium counter-ion to its adsorption on the mineral surface [84]. Despite its relatively more selective affinity than OHA for FA surface, BHA is known to be a weaker hydrophobing agent on Ca-bearing minerals, e.g., FA, compared to fatty acids and OHA [14,97,98]. The higher hydrophobing capability of OHA compared to BHA can be attributed to the establishment of more chain-chain interactions by OHA that favors the adsorption density. This will be further discussed later on in the following section through the experimental micro-flotation results. For fatty acid, despite its significant adsorption energies, it is adsorbed in lesser amount on the bare surface compared to HAs. This could be because fatty acids establish less chain-chain interaction, and therefore the formation of multi-layer adsorption is less favored despite high interaction energies of the functional head. As well, fatty acids have a higher packing area, and therefore the compacity of their adsorption layer is smaller [92,93]. On Al³⁺-treated FA (001) surface, at the first glance, it is seen that OHA preferentially adsorbs through a bidentate bonding of oxygen atoms of the functional group to the Al³⁺ cationic site at the treated surface. For SC, a bidentate bonding to both the Al³⁺ site as well as the Ca²⁺ lattice site is established. However, BHA unlike the other two reagents, prefers Ca²⁺ lattice cationic site over Al³⁺ to interact via a bidentate bonding. This is in line with the results of the adsorption density measurements where no considerable change in the BHA density of adsorption on the FA surface was observed when treated with Al³⁺. The adsorption energies of SC, OHA, and BHA molecules on the Al³⁺-treated FA surface were -431.4 (Al—O: 1.76 Å; Ca—O: 2.40 Å), -355.2 (Al—O: 1.98 Å), and -295.8 (Ca—O: 2.31 Å) kJ·mol⁻¹, as presented in Table 3. Hence, SC establishes a stronger and more favorable interaction with the Al³⁺-treated surface compared to the HA collectors.

Comparing the binding energies along with the Al—O bond lengths for the adsorption of SC and OHA molecules on the bare and Al³⁺-treated FA surface, the precipitation of Al-hydroxide on the FA surface is beneficial for the adsorption of these collectors. In the case of BHA, as noted earlier, the obtained visual configuration shows that the Al³⁺ site is not preferable for adsorption, whereas comparing the adsorption energies and configurations, it is obvious that BHA builds a stronger interaction with FA surface via a bidentate Ca—O bonding in the presence of Al-hydroxide. This could possibly be attributed to the influence of the effect of Al³⁺ metal ion on the FA mineral surface charge [28], as supported by the electro-kinetic measurements presented in Fig. 7, on

the BHA-FA interaction. A more thorough insight into this matter may deserve a distinct investigation, e.g., Bader charge analysis [99], which can be the focus of a future study by the authors. Besides, the sodium ion does not contribute to the adsorption of neither fatty acid nor HA molecules on the Al³⁺-treated FA surface and is substituted by the Al³⁺ ion as the counter-ion.

Looking at the adsorption configurations of the collector molecules on the Mg²⁺-treated FA surface, SC establishes a bidentate coordination bonding between two O⁻² ions of its carboxyl group and Mg²⁺ (Mg—O: 2.04 Å) as well as Ca²⁺ (Ca—O: 2.18 Å) cations on the treated surface. The adsorption energy of SC on the Mg²⁺-treated FA surface was -589.5 kJ·mol⁻¹, which speaks of a relatively more stable and stronger interaction. Comparing the bond lengths, it is evident that SC establishes a stronger interaction with Mg²⁺ than with Ca²⁺ ion, which can be attributed to the smaller size of magnesium ion [42,100]. This finding is consistent with the findings reported by Hirva and Tikka [101].

BHA and OHA adsorb on the Mg²⁺-treated FA surface through a bidentate coordination bonding between two O⁻² ions of their functional group and Ca²⁺ lattice cation (BHA: Ca—O: 2.21 Å; OHA: Ca—O: 2.26 Å) along with a mono-dentate bonding to the adsorbed Mg²⁺ site (BHA: Mg—O: 1.89 Å; OHA: Mg—O: 2.13 Å). Considering Mg—O and Ca—O bond lengths for SC, BHA and OHA, it can be speculated that the Mg bonding is stronger. Comparing these configurations with the mono-dentate adsorption of both BHA and OHA on the bare FA surface, it can be inferred that the adsorption of Mg²⁺ on the mineral surface increases the active cationic sites that interact with the functional groups of HA collectors, contributing to the improved FA floatability. The adsorption energies of BHA and OHA on the Mg²⁺-treated FA surface were -485.9 and -436.4 kJ mol⁻¹, which supports that BHA forms a stronger interaction with FA compared to OHA. On overall, fatty acid establishes a stronger interaction with the Mg²⁺-treated FA surface than the HA collectors. It is also shown that, in presence of Mg²⁺ adsorbed on the FA surface, sodium counter-ion does not contribute to the adsorption of either fatty acid or HA collectors and is substituted by Mg²⁺ as counter-ion.

As noted earlier, with regard to the coexistence of both the neutral and anionic forms of the HA collectors at pH 9, the adsorption mechanisms of the neutral HA collector molecules on bare and the treated FA surfaces were also investigated, and the results are presented in Fig. 11 and Table 3. The adsorption energies and configurations of the HA molecules in their neutral form on the FA surfaces were compared with those obtained for their anionic form accompanied by a sodium counter-ion (Fig. 10). It is seen that the HA molecules build stronger interactions with the mineral surface in their anionic form (more negative binding energies), which is consistent and further supported by the obtained Ca—O and/or Mg—O bond lengths. On the Al³⁺-treated surface, BHA under its anionic form establishes stronger Ca—O interaction by forming the bidentate bonding instead of the mono-dentate bonding in its neutral form. Similarly, for OHA, being in its anionic form brings about a bidentate Al—O interaction compared to the mono-dentate bonding with Al³⁺ site in its neutral form. Moreover, for both OHA and BHA on the Mg²⁺-treated surface, the anionic molecule forms a stronger interaction owed to the tridentate Ca—O and Mg—O bonding (Fig. 10) compared to the bidentate bonding of the neutral molecule with the mineral surface (Fig. 11). This is also supported by the shorter Ca—O/Mg—O bond lengths for the anionic molecule. From Fig. 11, it is also obvious that for the neutral molecules of the HA collectors, any adsorption configuration with either bare or treated surface is accompanied by a hydrogen bonding between an H atom of the HA to an O site at the FA surface, represented by a dashed line.

The adsorption energies for the target configurations, calculated by DFT calculations, are visually presented and compared with the corresponding adsorption densities obtained from the UV-Vis spectroscopy in Fig. 12. For the three target collectors under various scenarios except for BHA in the presence of Al³⁺, as discussed earlier, the amount of collector adsorbed on the mineral surface rises with a similar trend than the

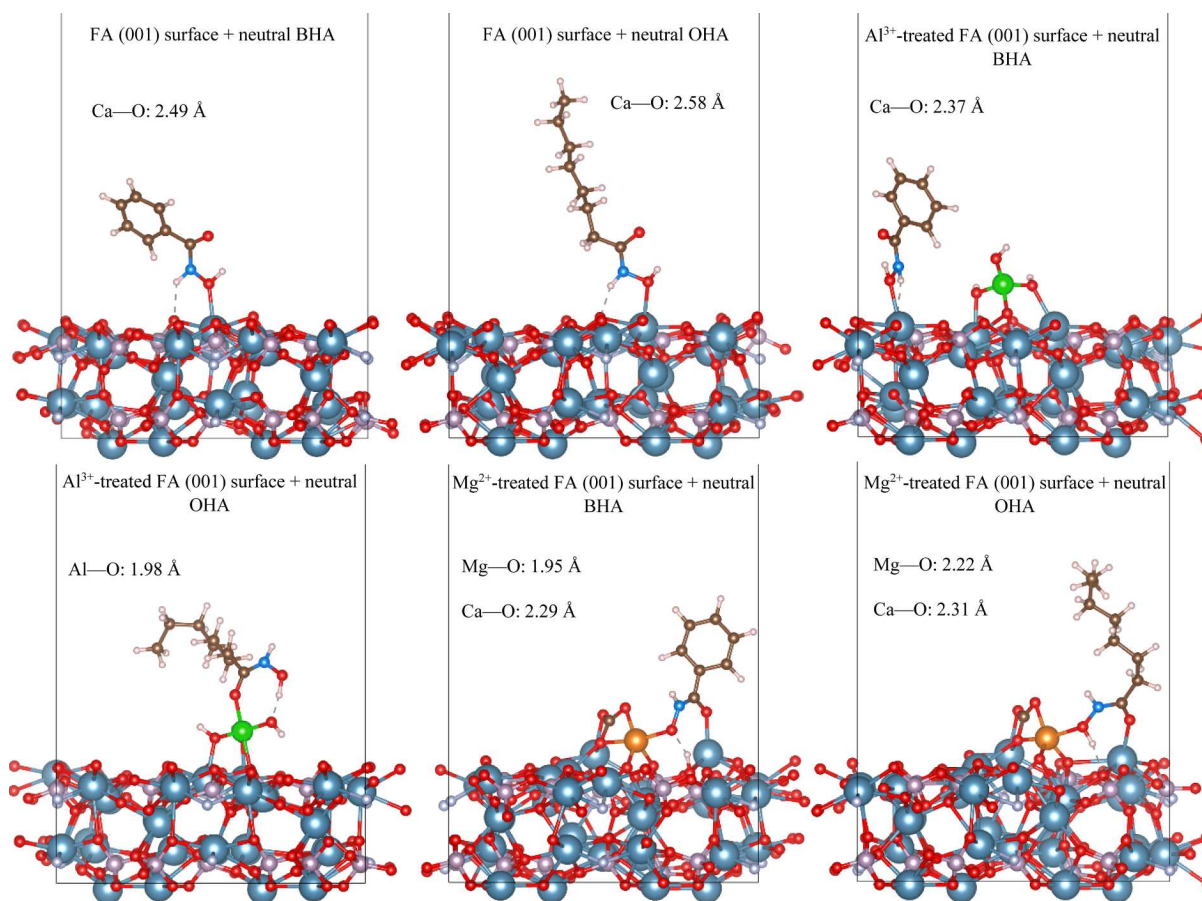


Fig. 11. Adsorption configurations of the neutral forms of the HA collectors on bare and $\text{Al}^{3+}/\text{Mg}^{2+}$ -treated (001) FA surface. The dashed lines indicate hydrogen bonds.

adsorption energy, which reveals a more stable and stronger collector-mineral interaction. On overall, the adsorption energies of the collectors are significantly correlated with the adsorption densities of these reagents on FA surface. This validates the use of adsorption energies to assess the stability of the adsorption layer on the mineral surfaces, and therefore their hydrophobation [102–104].

3.6. Micro-flotation tests

To assess how the obtained fundamental insights align with the froth flotation performance under the studied conditions and to assess the hydrophobicity of FA in the presence of the various collectors, micro-flotation experiments were conducted, and the results are presented in Fig. 13. For fatty acid collector, FA flotation recovery enhances in the presence of the metal ions following the order of $\text{Mg}^{2+} > \text{Al}^{3+}$. This is in line with the trend of the adsorption energies obtained from the DFT calculations, as shown in Fig. 13, as well as with the results of the adsorption density measurements presented in Fig. 9. First, this confirms that the adsorption energies of the collectors calculated by the atomistic simulations can be used to assess (1) their adsorption densities, and (2) the floatability/hydrophobicity of FA in the presence of these reagents. Second, these altogether confirm that the presence of Al^{3+} and Mg^{2+} metal ions in the flotation environment is beneficial for the flotation of FA using a fatty acid collector, with the latter being more favorable. For OHA, similarly to the fatty acid, FA flotation recovery increases, even though very slightly, in the presence of the metal ions in the order of $\text{Mg}^{2+} > \text{Al}^{3+}$. It is again consistent with the results of the adsorption density measurements (Fig. 9) and the adsorption energies as well as configurations obtained from the AIMD simulations, as compared in Fig. 13. For BHA, flotation recovery encounters respectively a decline

and a rise when Al^{3+} and Mg^{2+} metal ions are present in the solution compared to their absence, *i.e.*, in DI water. These results are in agreement with the results obtained for BHA from adsorption density measurements and AIMD simulations with a partial exception for the presence of Al^{3+} metal ions. The decline in the flotation recovery using BHA in the presence of Al^{3+} is consistent with the corresponding adsorption configuration obtained from AIMD simulations where it is shown that the BHA molecule prefers Ca^{2+} lattice sites over the Al^{3+} -treated site for adsorption. Adsorption density measurements also revealed that the presence of Al^{3+} ions does not benefit the amount of BHA adsorbed on the FA surface. However, the obtained adsorption energy for BHA on the Al^{3+} -treated FA surface does not coincide well with the experimental results, including both flotation recovery and adsorption density. This, as mentioned earlier, could possibly be attributed to the modified mineral surface charge due to the precipitation of Al-hydroxide species on the surface, as confirmed by the zeta potential measurements. A separate investigation, as noted earlier, into different aspects of this finding seems to be worthwhile. Moreover, considering the adsorption density measurements, AIMD simulations, and the flotation results, it is interesting to observe that the HA moiety behaves distinctively different towards Al^{3+} metal ions in the form of BHA and OHA compounds. This may raise the question of whether such discrepancy is induced by their class of hydrocarbon group, *i.e.*, aliphatic or aromatic. As known, BHA has an N-Hydroxybenzamide structure with benzamide being an aromatic amide, while OHA is an N-Hydroxyoctanamide compound with an octanamide as an aliphatic fatty acid amide [80]. The question, in other words, is if the chelating ability of HAs is influenced by their hydrocarbon group arrangement, especially with trivalent metals. This is yet to be explored in the context of froth flotation. Besides, the presence of the gangue metal ions in a flotation

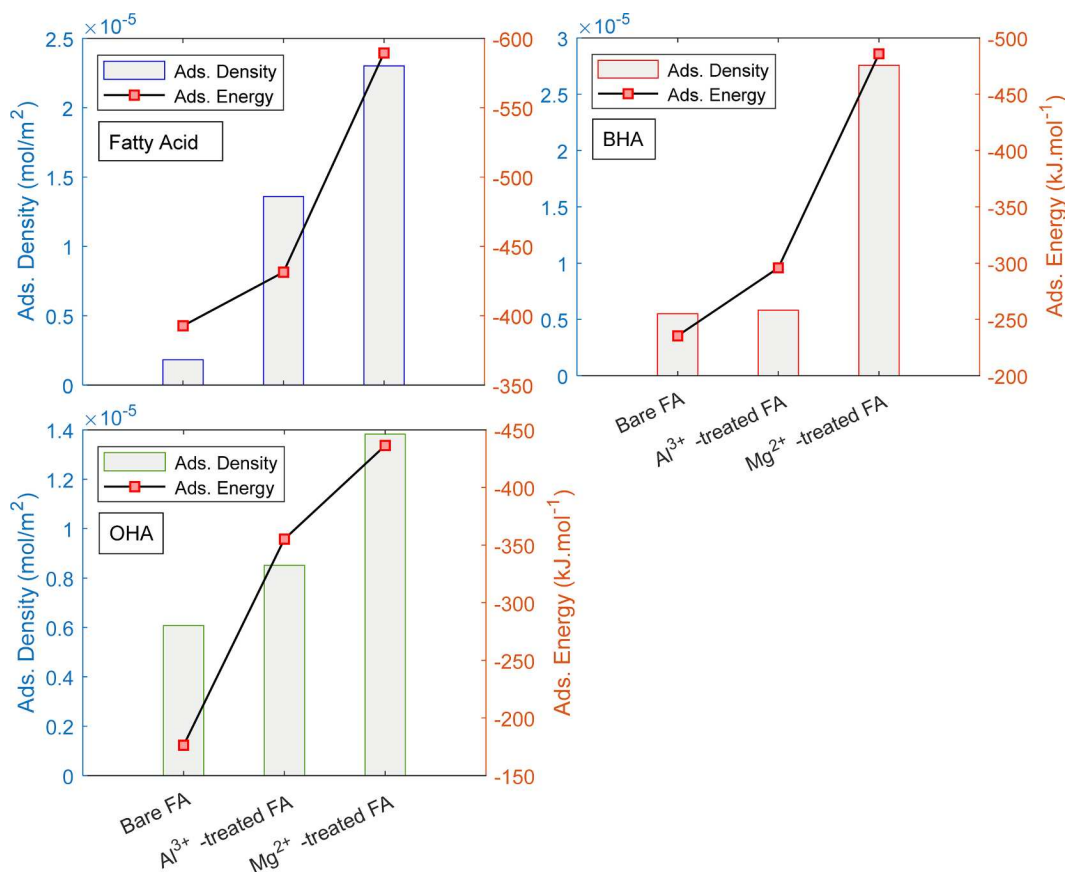


Fig. 12. The adsorption energies and densities for different collector molecules on the FA surface.

environment is linked to the presence of sparingly soluble gangue minerals. This, according to the results of the current study, means that a competitive consumption of the collector molecules available in the solution by both FA as the valuable and its associated gangue minerals that host these metal ions is unavoidable in a real flotation separation system. To that end, in order to obtain a more industrially applicable knowledge, different aspects of the effects of the metal ions on the flotation behavior of the gangue minerals for FA, e.g., dolomite, calcite, quartz, and clays in the presence of both fatty and hydroxamic acid collectors should also be investigated. This can develop the pathway to the design and development [105] of specially tailored reagents for the selective flotation of FA as the most characterized P-rich mineral from the troublesome low-grade secondary resources such as WC.

4. Conclusive remarks

This study aimed to unravel how the presence of Al³⁺ and Mg²⁺ metal ions influences the interaction of the collector reagents with the FA surface, and thereby its selective flotation performance. AIMD simulations helped understand interaction energies and adsorption configurations of both collectors and hydrolysis species of the metal ions with the mineral surface. Electro-kinetic measurements shed light on the surface charge modifications owed to the presence of the metal ions. XPS surface scanning revealed the type and the mechanism of the adsorption of the metal ions on the mineral surface. UV-Vis adsorption density measurements were conducted to determine the amount of the collector adsorbed on the mineral surface in the absence and presence of the metal ions. Finally, micro-flotation experiments showed how the fundamental experimental and theoretical insights would manifest in a real flotation environment. This study showed that:

- Fatty acid collector adsorbs on the bare FA surface through a bidentate Ca—O bonding along with a Na⁺-mediated O—O bonding. For the HA collectors, however, a mono-dentate Ca—O bonding is established.
- Na⁺ counter-ion contributes to the interaction of fatty acid collector with the bare FA surface via mediating the O—O bonding between the collector and the mineral surface.
- Fatty acid collector adsorbs on the Al³⁺-treated FA surface through the bidentate interaction with both adsorbed Al³⁺ and lattice Ca²⁺ ions through Al—O and Ca—O bonds, respectively.
- The presence of Al³⁺ results in a stronger OHA-mineral interaction through a bidentate Al—O bonding, and therefore an enhanced flotation performance. For BHA, however, the presence of Al³⁺ cations deteriorates the collector adsorption on the FA surface and thereby leads to a declined flotation performance.
- For fatty acid and HA collectors, the adsorption of Mg²⁺ species on the surface leads to the stronger mono-dentate and bidentate, respectively, Ca—O interaction of the collector molecule with a lattice Ca²⁺ ion along with a mono-dentate Mg—O bonding to the adsorbed Mg²⁺ site. BHA forms a stronger interaction with the FA surface in the presence of Mg²⁺ in comparison with OHA.
- Fatty acid collector establishes a more stable and stronger interaction with the bare as well as Al³⁺/Mg²⁺-treated FA mineral surface, as opposed to OHA and BHA.
- Both Al³⁺ and Mg²⁺ ions are beneficial for the adsorption of the fatty acid collector on the FA surface, and thereby its flotation. For both fatty acid and hydroxamates, Mg²⁺ is more favorable than Al³⁺ in apatite flotation.
- HA collectors build a stronger collector-mineral interaction with either bare or the treated FA surface in their free anionic form compared to their neutral form.

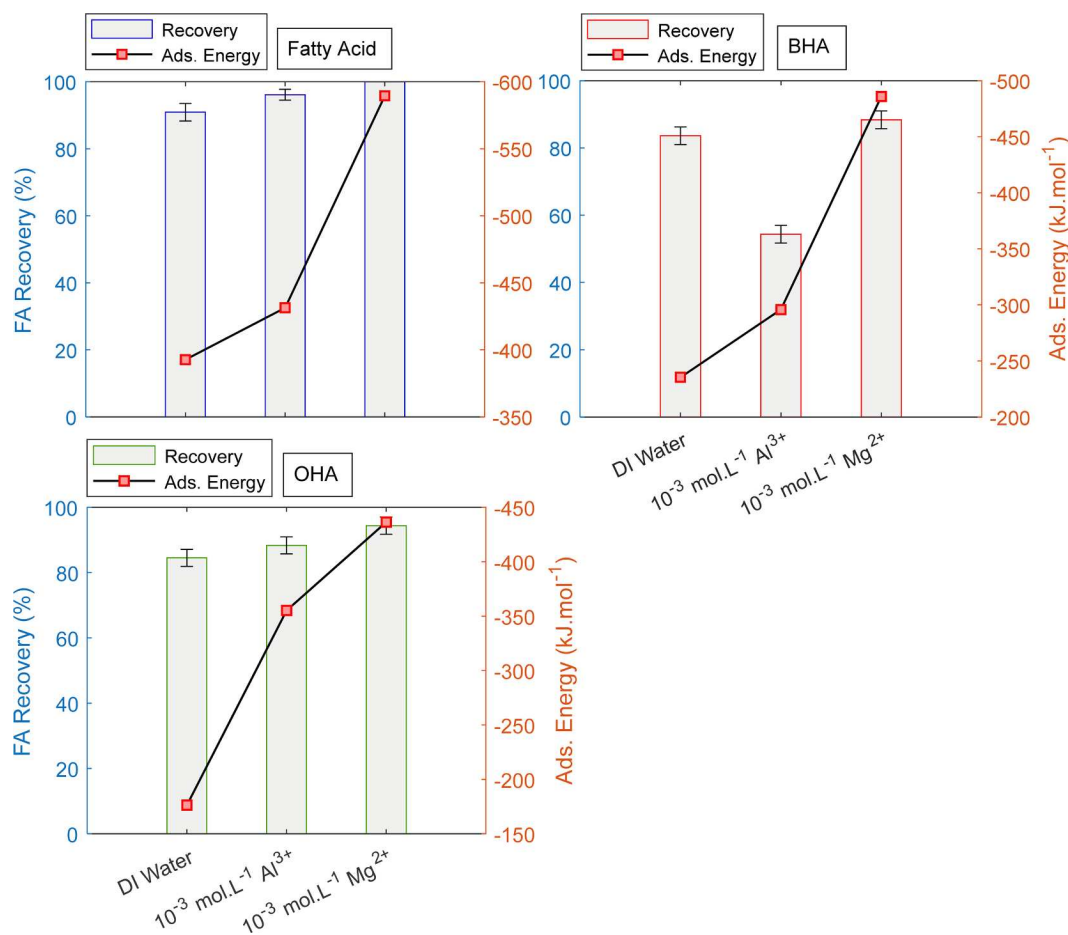


Fig. 13. Experimental FA flotation results compared with the theoretical adsorption energies for different collectors in the absence and presence of the metal ions.

- Interestingly, even though Al^{3+} deters the functionality of BHA on the FA surface, it contributes to a stronger BHA-mineral interaction through a bidentate Ca—O bonding. This could possibly be due to the modified mineral surface charge density owing to the precipitation of Al^{3+} species. In addition, such a discrepancy between the behavior of the two HA collectors towards the presence of Al^{3+} cations could be attributed to the type of the hydrocarbon group arrangement, *i.e.*, aliphatic or aromatic. It can be the focus of a separate study.
- A competitive consumption of the collector molecules by both FA and its gangues is inevitable during an actual flotation separation based on the current study's findings. Thus, in order to obtain a more industrially sound insight, the effects of the metal ions on the collector consumption by known grange minerals, and thereupon on the flotation selectivity should also be investigated in the future endeavors.

CRedit authorship contribution statement

Amir Eskanolou: Conceptualization, Data curation, Formal analysis, Investigation, Methodology, Validation, Visualization, Writing – original draft. **Qingqing Huang:** Conceptualization, Investigation, Funding acquisition, Project administration, Resources, Supervision, Validation, Visualization, Writing – review & editing. **Yann Foucaud:** Conceptualization, Data curation, Formal analysis, Investigation, Methodology, Validation, Visualization, Writing – review & editing. **Michael Badawi:** Data curation, Formal analysis, Methodology, Validation, Visualization, Writing – review & editing. **Aldo H. Romero:** Software, Writing – review & editing.

Declaration of Competing Interest

The authors declare that they have no known competing financial interests or personal relationships that could have appeared to influence the work reported in this paper.

Acknowledgements

We acknowledge the use of Thorny Flat High Performance Computing cluster, West Virginia University Research Computing (WVU-RC), and the use of the WVU Shared Research Facilities.

Appendix A. Supplementary material

Supplementary data to this article can be found online at <https://doi.org/10.1016/j.apsusc.2021.151499>.

References

- [1] Y. Pan, M.E. Fleet, Compositions of the apatite-group minerals: substitution mechanisms and controlling factors, *Rev. Mineral. Geochem.* 48 (1) (2002) 13–49.
- [2] S. Salvi, A.E. Williams-Jones, R.L. Linnen, I.M. Samson, Alkaline granite-syenite deposits, *Geological Association of Canada Short Course Notes* 17 (2005) 315–341.
- [3] S. Chander, D.W. Fuerstenau, Interfacial properties and equilibria in the apatite-aqueous solution system, *J. Colloid Interface Sci.* 70 (3) (1979) 506–516.
- [4] W. Cui, X. Song, J. Chen, Y. Chen, Y. Li, C. Zhao, Adsorption behaviors of different water structures on fluorapatite (001) surface: a DFT study, *Front. Mater.* 7 (2020).
- [5] N. Nan, Y. Zhu, Y. Han, J. Liu, Molecular modeling of interactions between N-(Carboxymethyl)-N-tetradecylglycine and fluorapatite, *Minerals* 9 (5) (2019) 278.

- [6] W. Forsling, L. Wu, Surface complexation at hydrous fluorapatite, *Aquat. Sci.* 55 (4) (1993) 336–346.
- [7] Y. Ruan, Z. Zhang, H. Luo, C. Xiao, F. Zhou, R. Chi, Effects of metal ions on the flotation of apatite, dolomite and quartz, *Minerals* 8 (4) (2018) 141.
- [8] M. Zeng, B. Yang, Z. Guan, L. Zeng, H. Luo, B. Deng, The selective adsorption of xanthan gum on dolomite and its implication in the flotation separation of dolomite from apatite, *Appl. Surf. Sci.* 551 (2021), 149301.
- [9] A. Eskanolou, M.R. Khalesi, M. Abdollahi, M. Hemmati Chegeni, Interactional effects of bubble size, particle size, and collector dosage on bubble loading in column flotation, *J. Mining Environ.* (1) (2018) 107–116.
- [10] B.A. Wills, J.A. Finch, *Froth Flotation. Wills' Mineral Processing Technology*, 8th ed., Butterworth-Heinemann, Boston, MA, 2016.
- [11] A. Eskanolou, B. Shahbazi, B. Vaziri Hassas, Estimation of flotation rate constant and collision efficiency using regression and artificial neural networks, *Sep. Sci. Technol.* 53 (2) (2018) 374–388.
- [12] M. Mohammadkhani, M. Noaparast, S.Z. Shafaei, A. Amini, E. Amini, H. Abdollahi, Double reverse flotation of a very low grade sedimentary phosphate rock, rich in carbonate and silicate, *Int. J. Miner. Process.* 100 (3–4) (2011) 157–165.
- [13] J.D. Miller, X. Wang, M. Li, October. Bench scale flotation of sedimentary phosphate rock with hydroxamic acid collectors, in: *Proceedings of the Engineering Foundation Conference, Beneficiation of Phosphates III: Fundamentals and Technology*, 2002, pp. 93–101.
- [14] L. Wang, M. Tian, S.A. Khoso, Y. Hu, W. Sun, Z. Gao, Improved flotation separation of apatite from calcite with benzohydroxamic acid collector, *Miner. Process. Extr. Metall. Rev.* 40 (6) (2019) 427–436.
- [15] M.C. Fuerstenau, *Chelating Agents as Flotation Collectors*, C. Young, JJ, 2005.
- [16] D.W. Fuerstenau, R. Herrera-Urbina, D.W. McGlashan, Studies on the applicability of chelating agents as universal collectors for copper minerals, *Int. J. Miner. Process.* 58 (1–4) (2000) 15–33.
- [17] K. Lee, D. Archibald, J. McLean, M.A. Reuter, Flotation of mixed copper oxide and sulphide minerals with xanthate and hydroxamate collectors, *Miner. Eng.* 22 (4) (2009) 395–401.
- [18] Y. Lu, S. Wang, H. Zhong, Study on the role of a hydroxamic acid derivative in wolframite flotation: selective separation and adsorption mechanism, *Appl. Surf. Sci.* 550 (2021), 149223.
- [19] R.H. Yoon, D.R. Nagaraj, S.S. Wang, T.M. Hildebrand, Beneficiation of kaolin clay by froth flotation using hydroxamate collectors, *Miner. Eng.* 5 (3–5) (1992) 457–467.
- [20] P. Zhang, H. Liang, Z. Jin, D. DePaoli, The ultimate mineral processing challenge: recovery of rare earths, phosphorus and uranium from Florida phosphatic clay, *Miner. Metall. Process.* 34 (4) (2017) 183–188.
- [21] J.G. McEvoy, Y. Thibault, Impact of crystal chemistry properties on the collector-mineral interactions observed for REE orthophosphates and oxides, *Appl. Surf. Sci.* 466 (2019) 970–981.
- [22] P. Zhang, R. Snow, Y. Yu, M. Bogan, Recovery of phosphate from Florida phosphatic clays, Final report, FIPR Publication, 2001, pp.02-096.
- [23] Amir Eskanolou, Qingqing Huang, Phosphatic waste clay: Origin, composition, physicochemical properties, challenges, values and possible remedies—A review, *Minerals Eng.* 162 (2021), 106745.
- [24] F. Zhou, Q. Liu, X. Liu, W. Li, J. Feng, R.A. Chi, Surface electrical behaviors of apatite, dolomite, quartz, and phosphate ore, *Front. Mater.* 7 (2020) 35, <https://doi.org/10.3389/fmats>.
- [25] M. Ejtemaei, M. Irannajad, M. Gharabaghi, Role of dissolved mineral species in selective flotation of smithsonite from quartz using oleate as collector, *Int. J. Miner. Process.* 114 (2012) 40–47.
- [26] C. Peng, Y. Zhong, G. Wang, F. Min, L. Qin, Atomic-level insights into the adsorption of rare earth Y(OH)_{3-n+} (n = 1–3) ions on kaolinite surface, *Appl. Surf. Sci.* 469 (2019) 357–367.
- [27] H.I.K.M.E.T. Sis, S. Chander, Reagents used in the flotation of phosphate ores: a critical review, *Miner. Eng.* 16 (7) (2003) 577–585.
- [28] F. Raji, M. Ejtemaei, A.V. Nguyen, Resolving the mystery of the second charge reversal on solid surfaces in the presence of divalent heavy metal ions, *Appl. Surf. Sci.* 529 (2020), 147128.
- [29] T.F. Al-Fariss, H.O. Ozbekelge, A.M. Abdulrazik, Flotation of a carbonate rich sedimentary phosphate rock, *Fertilizer Res.* 29 (2) (1991) 203–208.
- [30] D.G. Wonyen, V. Kromah, B. Gibson, S. Nah, S.C. Chelgani, A review of flotation separation of Mg carbonates (dolomite and magnesite), *Minerals* 8 (8) (2018) 354.
- [31] M.A. Dos Santos, R.C. Santana, F. Capponi, C.H. Ataíde, M.A. Barrozo, Effect of ionic species on the performance of apatite flotation, *Sep. Purif. Technol.* 76 (1) (2010) 15–20.
- [32] S. Al-Thyabat, H. Al-Zoubi, Purification of phosphate beneficiation wastewater: Separation of phosphate from Eshydia Mine (Jordan) by column-DAF flotation process, *Int. J. Miner. Process.* 110 (2012) 18–24.
- [33] D.A. Elgillani, A.Z. Abouzeid, Flotation of carbonates from phosphate ores in acidic media, *Int. J. Miner. Process.* 38 (3–4) (1993) 235–256.
- [34] H.I.K.M.E.T. Sis, S. Chander, Adsorption and contact angle of single and binary mixtures of surfactants on apatite, *Miner. Eng.* 16 (9) (2003) 839–848.
- [35] X. Liu, C. Li, H. Luo, R. Cheng, F. Liu, Selective reverse flotation of apatite from dolomite in colophonite ore using sulfonated gutter oil fatty acid as a collector, *Int. J. Miner. Process.* 165 (2017) 20–27.
- [36] D. Horta, M.B. de Mello Monte, The effect of dissolution kinetics on flotation response of apatite with sodium oleate, *Int. J. Miner. Process.* 146 (2016) 97–104.
- [37] H. Jabraoui, E.P. Hessou, S. Chibani, L. Cantrel, S. Lebègue, M. Badawi, Adsorption of volatile organic and iodine compounds over silver-exchanged mordenites: a comparative periodic DFT study for several silver loadings, *Appl. Surf. Sci.* 485 (2019) 56–63.
- [38] Y. Foucaud, M. Badawi, L. Filippov, I. Filippova, S. Lebègue, A review of atomistic simulation methods for surface physical-chemistry phenomena applied to froth flotation, *Miner. Eng.* 143 (2019), 106020.
- [39] Y. Foucaud, R.L.S. Canevesi, A. Celzard, V. Fierro, M. Badawi, Hydration mechanisms of scheelite from adsorption isotherms and ab initio molecular dynamics simulations, *Appl. Surf. Sci.* 562 (2021), 150137.
- [40] D. Mkhonto, P.E. Ngoepe, T.G. Cooper, N.H. de Leeuw, A computer modelling study of the interaction of organic adsorbates with fluorapatite surfaces, *Phys. Chem. Miner.* 33 (5) (2006) 314–331.
- [41] J. Xie, X. Li, S. Mao, L. Li, B. Ke, Q. Zhang, Effects of structure of fatty acid collectors on the adsorption of fluorapatite (001) surface: A first-principles calculations, *Appl. Surf. Sci.* 444 (2018) 699–709.
- [42] I.V. Filippova, L.O. Filippov, Z. Lafhaj, O. Barres, D. Fornasiero, Effect of calcium minerals reactivity on fatty acids adsorption and flotation, *Colloids Surf., A* 545 (2018) 157–166.
- [43] R. Zheng, Z. Ren, H. Gao, Z. Chen, Y. Qian, Y. Li, Effects of crystal chemistry on sodium oleate adsorption on fluorite surface investigated by molecular dynamics simulation, *Miner. Eng.* 124 (2018) 77–85.
- [44] P. Rulis, H. Yao, L. Ouyang, W.Y. Ching, Electronic structure, bonding, charge distribution, and x-ray absorption spectra of the (001) surfaces of fluorapatite and hydroxyapatite from first principles, *Phys. Rev. B* 76 (24) (2007), 245410.
- [45] B. Pavan, D. Ceresoli, M.M. Tecklenburg, M. Fornari, First principles NMR study of fluorapatite under pressure, *Solid State Nucl. Magn. Reson.* 45 (2012) 59–65.
- [46] X. Wang, Q. Zhang, S. Mao, W. Cheng, A theoretical study on the electronic structure and floatability of rare earth elements (La, Ce, Nd and Y) bearing fluorapatite, *Minerals* 9 (8) (2019) 500.
- [47] C. Chairat, J. Schott, E.H. Oelkers, J.E. Lartigue, N. Harouiya, Kinetics and mechanism of natural fluorapatite dissolution at 25 °C and pH from 3 to 12, *Geochim. Cosmochim. Acta* 71 (24) (2007) 5901–5912.
- [48] K.H. Rao, B.M. Antti, E. Forssberg, Mechanism of oleate interaction on salt-type minerals, Part II. Adsorption and electrokinetic studies of apatite in the presence of sodium oleate and sodium metasilicate, *Int. J. Miner. Process.* 28 (1–2) (1990) 59–79.
- [49] J. Nduwa-Mushidi, C.G. Anderson, Surface chemistry and flotation behaviors of monazite-apatite-ilmenite-quartz-rutile-zircon with octanohydroxamic acid, *J. Sustain. Metall.* 3 (1) (2017) 62–72.
- [50] P. Villars, K. Cenzual, H. Okamoto, F. Hulliger, S. Iwata, *PAULING FILE Multinaries Edition-2012*, 2012.
- [51] S.V. Dorozhkin, Dissolution mechanism of calcium apatites in acids: a review of literature, *World J. Methodol.* 2 (1) (2012) 1.
- [52] T.J. White, Z. Dong, Structural derivation and crystal chemistry of apatites, *Acta Crystallogr. B* 59 (1) (2003) 1–16.
- [53] J.M. Hughes, J. Rakovan, 1. The Crystal Structure of Apatite, Ca₅(PO₄)₃(F, OH, Cl), *Phosphates*, 2018, pp. 1–12.
- [54] J.M. Hughes, The many facets of apatite, *Am. Mineral.* 100 (5–6) (2015) 1033–1039.
- [55] E.C. Moreno, M. Kresak, R.T. Zahradnik, Fluoridated hydroxyapatite solubility and caries formation, *Nature* 247 (5435) (1974) 64–65.
- [56] C. Rey, C. Combes, C. Drouet, H. Sfihi, Fluoride-based bioceramics, in: *Fluorine and Health*, Elsevier, 2008, pp. 279–331.
- [57] K.A. Chin, G.H. Nancollas, Dissolution of fluorapatite. A constant-composition kinetics study, *Langmuir* 7 (10) (1991) 2175–2179.
- [58] S.V. Dorozhkin, Surface reactions of apatite dissolution, *J. Colloid Interface Sci.* 191 (2) (1997) 489–497.
- [59] O. Hochrein, D. Zahn, On the molecular mechanisms of the acid-induced dissociation of hydroxy-apatite in water, *J. Mol. Model.* 17 (6) (2011) 1525–1528.
- [60] S. Broom-Fendley, M.T. Styles, J.D. Appleton, G. Gunn, F. Wall, Evidence for dissolution-reprecipitation of apatite and preferential LREE mobility in carbonate-derived late-stage hydrothermal processes, *Am. Mineral.* 101 (3) (2016) 596–611.
- [61] P. Ptáček, Substituents and dopants in the structure of apatite. Apatites and their synthetic analogues—synthesis, structure, properties and applications. InTech, Open Access monograph, 2016, pp. 289–334.
- [62] J.N. Israelachvili, Electrostatic forces between surfaces in liquids, *Intermol. Surf. Forces* 3 (2011) 291–340.
- [63] A. Eskanolou, Q. Huang, M.H. Chegeni, M.R. Khalesi, M. Abdollahi, Determination of the mass transfer rate constant in a laboratory column flotation using the bubble active surface coefficient, *Miner. Eng.* 156 (2020), 106521.
- [64] Y. Foucaud, M. Badawi, L.O. Filippov, O. Barres, I.V. Filippova, S. Lebègue, Synergistic adsorptions of Na₂CO₃ and Na₂SiO₃ on calcium minerals revealed by spectroscopic and ab initio molecular dynamics studies, *Chem. Sci.* 10 (43) (2019) 9928–9940.
- [65] C.D. Wagner, Photoelectron and Auger energies and the Auger parameter: a data set, *Practical surface analysis*, 1990.
- [66] S.B. Hendricks, M.E. Jefferson, V.M. Mosley, The crystal structures of some natural and synthetic apatite-like substances, *Zeitschrift für Kristallographie-Crystalline Materials* 81 (1–6) (1932) 352–369.
- [67] G. Kresse, J. Hafner, Ab initio molecular dynamics for liquid metals, *Phys. Rev. B* 47 (1) (1993) 558.
- [68] J.P. Perdew, K. Burke, M. Ernzerhof, Generalized gradient approximation made simple, *Phys. Rev. Lett.* 77 (18) (1996) 3865.
- [69] W. Kohn, L.J. Sham, Self-consistent equations including exchange and correlation effects, *Phys. Rev.* 140 (4A) (1965) A1133.

- [70] G. Kresse, J. Furthmüller, Efficient iterative schemes for ab initio total-energy calculations using a plane-wave basis set, *Phys. Rev. B* 54 (16) (1996) 11169.
- [71] G. Kresse, D. Joubert, From ultrasoft pseudopotentials to the projector augmented-wave method, *Phys. Rev. B* 59 (3) (1999) 1758.
- [72] M.P.A.T. Methfessel, A.T. Paxton, High-precision sampling for Brillouin-zone integration in metals, *Phys. Rev. B* 40 (6) (1989) 3616.
- [73] K. Georg, VASP Group, Theoretical Physics Departments, Vienna. Retrieved February, 21, 2011.
- [74] J. Xie, Q. Zhang, S. Mao, X. Li, Z. Shen, L. Li, Anisotropic crystal plane nature and wettability of fluorapatite, *Appl. Surf. Sci.* 493 (2019) 294–307.
- [75] S. Nosé, A molecular dynamics method for simulations in the canonical ensemble, *Mol. Phys.* 52 (2) (1984) 255–268.
- [76] S. Nosé, A unified formulation of the constant temperature molecular dynamics methods, *J. Chem. Phys.* 81 (1) (1984) 511–519.
- [77] W.G. Hoover, Canonical dynamics: equilibrium phase-space distributions, *Phys. Rev. A* 31 (3) (1985) 1695.
- [78] Y. Foucaud, S. Lebègue, L.O. Filippov, I.V. Filippova, M. Badawi, Molecular insight into fatty acid adsorption on bare and hydrated (111) fluorite surface, *J. Phys. Chem. B* 122 (51) (2018) 12403–12410.
- [79] M.M. Khalil, R.K. Mahmoud, New insights into M(II)–hydroxamate interactions: the electro-analytical behavior of metal (II) complexes involving monohydroxamic acids and diamines in an aqueous medium, *J. Chem. Eng. Data* 53 (10) (2008) 2318–2327.
- [80] <https://www.pubchem.ncbi.nlm.nih.gov/>.
- [81] Z. Danna, Applications of Chemical Equilibrium Diagram Software HYDRA/MEDUSA in Teaching College Chemistry, University Chemistry, 2015, p. 04.
- [82] Gilbert, A.T.B., 2012. IQmol molecular viewer; <http://iqmol.org>; accessed 27 May 2021.
- [83] M.D. Hanwell, D.E. Curtis, D.C. Lonie, T. Vandermeersch, E. Zurek, G. R. Hutchison, Avogadro: an advanced semantic chemical editor, visualization, and analysis platform, *J. Cheminf.* 4 (1) (2012) 1–17.
- [84] Y. Foucaud, J. Lainé, L.O. Filippov, O. Barrès, W.J. Kim, I.V. Filippova, M. Pastore, S. Lebègue, M. Badawi, Adsorption mechanisms of fatty acids on fluorite unraveled by infrared spectroscopy and first-principles calculations, *J. Colloid Interface Sci.* 583 (2021) 692–703.
- [85] K. Momma, F. Izumi, VESTA 3 for three-dimensional visualization of crystal, volumetric and morphology data, *J. Appl. Crystallogr.* 44 (6) (2011) 1272–1276.
- [86] O. Paulson, R.J. Pugh, Flotation of inherently hydrophobic particles in aqueous solutions of inorganic electrolytes, *Langmuir* 12 (20) (1996) 4808–4813.
- [87] B. Vaziri Hassas, S. Kouachi, A. Eskanolou, M. Bouhenguel, M.S. Çelik, J.D. Miller, The significance of positive and negative inertial forces in Particle-Bubble interaction and their role in the general flotation kinetics model, *Miner. Eng.* 170 (2021), 107006.
- [88] J.O. Amankonah, P. Somasundaran, K.P. Ananthapadmbhan, Effects of dissolved mineral species on the dissolution/precipitation characteristics of calcite and apatite, *Colloids Surf.* 15 (1985) 295–307.
- [89] J. Chastain, R.C. King Jr, Handbook of X-ray photoelectron spectroscopy, Perkin-Elmer Corporation 40 (1992) 221.
- [90] A. Geneyton, Y. Foucaud, L.O. Filippov, N.E. Menad, A. Renard, M. Badawi, Synergistic adsorption of lanthanum ions and fatty acids for efficient rare-earth phosphate recovery: surface analysis and ab initio molecular dynamics studies, *Appl. Surf. Sci.* 526 (2020), 146725.
- [91] X. Liu, Y. Zhao, Q. Li, T. Jiao, J. Niu, Adsorption behavior, spreading and thermal stability of anionic-nonionic surfactants with different ionic headgroup, *J. Mol. Liq.* 219 (2016) 1100–1106.
- [92] L. Xu, J. Tian, H. Wu, Z. Lu, W. Sun, Y. Hu, The flotation and adsorption of mixed collectors on oxide and silicate minerals, *Adv. Colloid Interface Sci.* 250 (2017) 1–14.
- [93] K.T. Nguyen, T.D. Nguyen, A.V. Nguyen, Strong cooperative effect of oppositely charged surfactant mixtures on their adsorption and packing at the air–water interface and interfacial water structure, *Langmuir* 30 (24) (2014) 7047–7051.
- [94] T.A. Albright, J.K. Burdett, M.H. Whangbo, *Orbital Interactions in Chemistry*, John Wiley & Sons, 2013.
- [95] P. Somasundaran, J.O. Amankonah, K.P. Ananthapadmbhan, Mineral-solution equilibria in sparingly soluble mineral systems, *Colloids Surf.* 15 (1985) 309–333.
- [96] C.L. Owens, G.R. Nash, K. Hadler, R.S. Fitzpatrick, C.G. Anderson, F. Wall, Apatite enrichment by rare earth elements: a review of the effects of surface properties, *Adv. Colloid Interface Sci.* 265 (2019) 14–28.
- [97] W. Jiang, Z. Gao, S.A. Khoso, J. Gao, W. Sun, W. Pu, Y. Hu, Selective adsorption of benzhydroxamic acid on fluorite rendering selective separation of fluorite/calcite, *Appl. Surf. Sci.* 435 (2018) 752–758.
- [98] N. Kupka, M. Rudolph, Froth flotation of scheelite—a review, *Int. J. Mining Sci. Technol.* 28 (3) (2018) 373–384.
- [99] R.F.W. Bader, *Atoms in Molecules: A Quantum Theory*, Oxford University Press, Oxford, UK, 1990.
- [100] P. Somasundaran, L. Zhang, Reagent adsorption on phosphates, *Encyclopedia of Separation Science* 4 (2000).
- [101] P. Hirva, H.K. Tikka, Ab initio study on the interaction of anionic collectors with calcite and dolomite surfaces, *Langmuir* 18 (12) (2002) 5002–5006.
- [102] S.K. Solongo, A. Gomez-Flores, J. You, S. Choi, G.W. Heyes, S. Ilyas, J. Lee, H. Kim, Cationic collector conformations on an oxide mineral interface: Roles of pH, ionic strength, and ion valence, *Miner. Eng.* 150 (2020), 106277.
- [103] A. Eskanolou, M.H. Chegeni, M.R. Khalesi, M. Abdollahy, Q. Huang, Modeling the bubble loading based on force balance on the particles attached to the bubble, *Colloids Surf., A* 582 (2019), 123892.
- [104] A. Eskanolou, M.R. Khalesi, M. Abdollahy, Bubble loading profiles in a flotation column, *Physicochem. Problems Mineral Process.* 54 (2018).
- [105] G. Liu, X. Yang, H. Zhong, Molecular design of flotation collectors: a recent progress, *Adv. Colloid Interface Sci.* 246 (2017) 181–195.